

High pressure crystallization of long chain branched polypropylene

Bc. Lukáš Kovář

Master thesis
2010



Tomas Bata University in Zlín
Faculty of Technology

Univerzita Tomáše Bati ve Zlíně

Fakulta technologická

Ústav inženýrství polymerů

akademický rok: 2009/2010

ZADÁNÍ DIPLOMOVÉ PRÁCE

(PROJEKTU, UMĚLECKÉHO DÍLA, UMĚLECKÉHO VÝKONU)

Jméno a příjmení: **Bc. Lukáš KOVÁŘ**

Studijní program: **N 2808 Chemie a technologie materiálů**

Studijní obor: **Inženýrství polymerů**

Téma práce: **Vysokotlaká krystalizace větveného polypropylenu**

Zásady pro vypracování:

The aim of this Master thesis is to study crystallization of long chain branched polypropylene (LCB PP) under increased pressure. The introduction of long chain branching onto polypropylene backbone leads to improvement of melt strength and thus the material is suitable for otherwise limiting processing such as thermoforming, foaming and blow molding. However, the change of molecular architecture can affect not only rheological properties but also crystallization of PP. Moreover, the pressure which is often applied during processing can play an important role as it causes the crystallization into orthorhombic γ -phase. This polymorph of isotactic polypropylene possesses different physical properties than common monoclinic α -phase, e. g. lower opacity. In the work, LCB PP and also standard PP will be crystallized under several pressures. Then, the structure will be evaluated via several methods such as X-ray scattering, differential scanning calorimetry, optical microscopy and scanning electron microscopy and mechanical properties testing.

Rozsah práce:

Rozsah příloh:

Forma zpracování diplomové práce: **tisková/elektronická**

Seznam odborné literatury:

1. Karger-Kocsis, J.: Polypropylene – An A-Z Reference, Springer – Verlag, 1999, ISBN: 0-412-80200-7

2. Maier, C.; Calafut, T.: Polypropylene – The Definitive User's Guide and Databook, William Andrew Publishing/Plastics Design Library, 1998, ISBN: 1-884207-58-8 and scientific articles

Vedoucí diplomové práce:

Ing. Jana Navrátilová, Ph.D.

Ústav inženýrství polymerů

Datum zadání diplomové práce:

15. února 2010


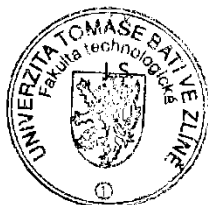
Termín odevzdání diplomové práce:

14. května 2010

Ve Zlíně dne 15. února 2010



doc. Ing. Petr Hlaváček, CSc.
děkan



doc. Ing. Roman Čermák, Ph.D.
ředitel ústavu

Příjmení a jméno: Kovář Lukáš

Obor: Inženýrství polymerů

PROHLÁŠENÍ

Prohlašuji, že

- beru na vědomí, že odevzdáním diplomové/bakalářské práce souhlasím se zveřejněním své práce podle zákona č. 111/1998 Sb. o vysokých školách a o změně a doplnění dalších zákonů (zákon o vysokých školách), ve znění pozdějších právních předpisů, bez ohledu na výsledek obhajoby¹⁾;
- beru na vědomí, že diplomová/bakalářská práce bude uložena v elektronické podobě v univerzitním informačním systému dostupná k nahlédnutí, že jeden výtisk diplomové/bakalářské práce bude uložen na příslušném ústavu Fakulty technologické UTB ve Zlíně a jeden výtisk bude uložen u vedoucího práce;
- byl/a jsem seznámen/a s tím, že na moji diplomovou/bakalářskou práci se plně vztahuje zákon č. 121/2000 Sb. o právu autorském, o právech souvisejících s právem autorským a o změně některých zákonů (autorský zákon) ve znění pozdějších právních předpisů, zejm. § 35 odst. 3²⁾;
- beru na vědomí, že podle § 60³⁾ odst. 1 autorského zákona má UTB ve Zlíně právo na uzavření licenční smlouvy o užití školního díla v rozsahu § 12 odst. 4 autorského zákona;
- beru na vědomí, že podle § 60³⁾ odst. 2 a 3 mohu užít své dílo – diplomovou/bakalářskou práci nebo poskytnout licenci k jejímu využití jen s předchozím písemným souhlasem Univerzity Tomáše Bati ve Zlíně, která je oprávněna v takovém případě ode mne požadovat přiměřený příspěvek na úhradu nákladů, které byly Univerzitou Tomáše Bati ve Zlíně na vytvoření díla vynaloženy (až do jejich skutečné výše);
- beru na vědomí, že pokud bylo k vypracování diplomové/bakalářské práce využito softwaru poskytnutého Univerzitou Tomáše Bati ve Zlíně nebo jinými subjekty pouze ke studijním a výzkumným účelům (tedy pouze k nekomerčnímu využití), nelze výsledky diplomové/bakalářské práce využít ke komerčním účelům;
- beru na vědomí, že pokud je výstupem diplomové/bakalářské práce jakýkoliv softwarový produkt, považují se za součást práce rovněž i zdrojové kódy, popř. soubory, ze kterých se projekt skládá. Neodevzdání této součásti může být důvodem k neobhájení práce.

Ve Zlíně 7. 5. 2010


.....

¹⁾ zákon č. 111/1998 Sb. o vysokých školách a o změně a doplnění dalších zákonů (zákon o vysokých školách), ve znění pozdějších právních předpisů, § 47 Zveřejňování závěrečných prací:

(1) Vysoká škola nevydělečně zveřejňuje disertační, diplomové, bakalářské a rigorózní práce, u kterých proběhla obhajoba, včetně posudků oponentů a výsledku obhajoby prostřednictvím databáze kvalifikačních prací, kterou spravuje. Způsob zveřejnění stanoví vnitřní předpis vysoké školy.

(2) Disertační, diplomové, bakalářské a rigorózní práce odevzdané uchazečem k obhajobě musí být též nejméně pět pracovních dnů před konáním obhajoby zveřejněny k nahlížení veřejnosti v místě určeném vnitřním předpisem vysoké školy nebo není-li tak určeno, v místě pracoviště vysoké školy, kde se má konat obhajoba práce. Každý si může ze zveřejněné práce pořizovat na své náklady výpisy, opisy nebo rozmnoženiny.

(3) Platí, že odevzdáním práce autor souhlasí se zveřejněním své práce podle tohoto zákona, bez ohledu na výsledek obhajoby.

²⁾ zákon č. 121/2000 Sb. o právu autorském, o právech souvisejících s právem autorským a o změně některých zákonů (autorský zákon) ve znění pozdějších právních předpisů, § 35 odst. 3:

(3) Do práva autorského také nezasahuje škola nebo školské či vzdělávací zařízení, užije-li nikoli za účelem přímého nebo nepřímého hospodářského nebo obchodního prospěchu k výuce nebo k vlastní potřebě dílo vytvořené žákem nebo studentem ke splnění školních nebo studijních povinností vyplývajících z jeho právního vztahu ke škole nebo školskému či vzdělávacímu zařízení (školní dílo).

³⁾ zákon č. 121/2000 Sb. o právu autorském, o právech souvisejících s právem autorským a o změně některých zákonů (autorský zákon) ve znění pozdějších právních předpisů, § 60 Školní dílo:

(1) Škola nebo školské či vzdělávací zařízení mají za obvyklých podmínek právo na uzavření licenční smlouvy o užití školního díla (§ 35 odst. 3). Odpírá-li autor takového díla udělit svolení bez vážného důvodu, mohou se tyto osoby domáhat nahrazení chybějícího projevu jeho vůle u soudu. Ustanovení § 35 odst. 3 zůstává nedotčeno.

(2) Není-li sjednáno jinak, může autor školního díla své dílo užít či poskytnout jinému licenci, není-li to v rozporu s oprávněnými zájmy školy nebo školského či vzdělávacího zařízení.

(3) Škola nebo školské či vzdělávací zařízení jsou oprávněny požadovat, aby jim autor školního díla z výdělku jím dosaženého v souvislosti s užitím díla či poskytnutím licence podle odstavce 2 přiměřeně přispěl na úhradu nákladů, které na vytvoření díla vynaložily, a to podle okolností až do jejich skutečné výše; přitom se přihlédne k výši výdělku dosaženého školou nebo školským či vzdělávacím zařízením z užití školního díla podle odstavce 1.

ABSTRAKT

Cílem diplomové práce je studium krystalizace a morfologie polypropylenu s dlouhými bočními větvemi (LCB-PP) za zvýšeného tlaku. Zavedení dlouhých bočních větví na kostru polypropylenu (PP) vede ke zvýšení pevnosti taveniny a materiál je vhodnější pro zpracovatelské procesy jako tvarování, zpěňování a vyfukování. LCB-PP má větší tendenci krystalizovat do γ -formy pod tlakem. V této práci byly podrobeny krystalizaci pod různými tlaky materiály LCB-PP, lineární PP s podobným indexem toku taveniny, a také PP o velmi vysoké čistotě zbavený katalytických zbytků.

Struktura uvedených materiálů byla v práci zkoumána pomocí širokouhlé rentgenografie, diferenciální snímání kalorimetrie, skenovací elektronové mikroskopie a mechanické vlastnosti byly stanoveny tlakovou zkouškou. Byla potvrzena zvýšená tendence tvorby γ -fáze u LCB-PP.

Klíčová slova: vysokotlaká krystalizace, polypropylen s dlouhými bočními větvemi, širokouhlá rentgenografie, diferenciální snímání kalorimetrie, skenovací elektronová mikroskopie, tlaková zkouška.

ABSTRACT

The aim of the Master thesis is to study crystallization and morphology of long chain branched polypropylene (LCB-PP) under increased pressure. The introduction of long chain branching onto polypropylene (PP) backbone leads to improvement of melt strength and thus the material is suitable for otherwise limiting processing such as thermoforming, foaming and blow molding. LCB-PP has higher tendency to form orthorombic γ -form under pressure. In this work LCB-PP, common linear PP with similar melt flow index and also PP which was cleaned to eliminate catalyst residues were crystallized under several pressures.

Then, the structure was evaluated via several methods, namely wide angle X-ray scattering, differential scanning calorimetry, scanning electron microscopy. Mechanical properties were determined via compressive testing. The higher tendency to crystallize into γ -form in LCB-PP was proved.

Keywords: high pressure crystallization, long chain branched polypropylene, wide angle X-ray scattering, differential scanning calorimetry, scanning electron microscopy, compressive testing.

ACKNOWLEDGEMENTS

I would like to express my sincere gratitude to Ing. Jana Navrátilová, Ph.D. for her supervision, support with valuable advices, collecting information, express my ideas, correcting grammar and help with experiments, that have helped me to complete this Master thesis.

Also I would like to thank to all the people who helped me with experiments and gave me valuable advices.

Finally, an honorable mention goes to my family for understanding and support on me in completing this project.

I hereby declare that the print version of my Master's thesis and the electronic version of my thesis deposited in the IS/STAG system are identical.

Zlín, 7.May 2010



Lukáš Kovář

CONTENTS

INTRODUCTION	10
I THEORETICAL PART	12
1 CRYSTALLIZATION OF POLYMERS.....	13
1.1 NUCLEATION	13
1.2 CRYSTAL GROWTH	14
1.3 MORPHOLOGY OF CRYSTALLINE POLYMERS	15
1.3.1 Single Lamellae.....	15
1.3.2 Spherulites.....	16
1.4 CRYSTALLIZATION UNDER HIGH PRESSURE	18
1.4.1 Avrami equation.....	18
1.4.2 Formation of γ -form of iPP	19
2 POLYPROPYLENE	20
2.1 POLYMERIZATION	20
2.2 CHEMICAL STRUCTURE.....	20
2.2.1 Isotactic polypropylene	21
2.2.2 Syndiotactic polypropylene.....	21
2.2.3 Atactic polypropylene	21
2.3 POLYMORPHISM OF ISOTACTIC POLYPROPYLENE.....	22
2.3.1 α -form.....	23
2.3.2 β -form.....	24
2.3.3 γ -form	25
2.4 PROPERTIES AND APPLICATIONS OF POLYPROPYLENE.....	26
2.5 LONG CHAIN BRANCHED POLYPROPYLENE	26
2.5.1 Polymerization	27
2.5.2 Crystallization	31
2.5.3 Properties.....	32
2.5.4 Application.....	33
3 METHODS OF ANALYSIS.....	35
3.1 WIDE ANGLE X-RAY SCATTERING	35
3.2 SCANNING ELECTRON MICROSCOPY	36
3.3 DIFFERENTIAL SCANNING CALORIMETRY	37
3.4 DETERMINATION OF COMPRESSIVE PROPERTIES (ČSN EN ISO 604).....	39
II EXPERIMENTAL PART	41
4 MATERIALS AND SAMPLE PREPARATION	42
4.1 SPECIMENS FOR WIDE ANGLE X-RAY SCATTERING	44
4.2 SPECIMENS FOR SCANNING ELECTRON MICROSCOPY	45
4.3 SPECIMENS FOR DSC ANALYSIS	45
4.4 SPECIMENS FOR DETERMINATION OF COMPRESSIVE PROPERTIES	45

5	ANALYZING METHODS AND DEVICES.....	46
5.1	WIDE ANGLE X-RAY SCATTERING	46
5.2	DIFFERENTIAL SCANNING CALORIMETRY ANALYSIS.....	46
5.3	SCANNING ELECTRON MICROSCOPY	47
5.4	COMPRESSIVE TESTING.....	48
III	RESULTS AND DISCUSSION	49
6	HIGH PRESSURE CRYSTALLIZATION	50
7	WIDE ANGLE X-RAY SCATTERING	53
8	DIFFERENTIAL SCANNING CALORIMETRY.....	57
9	SCANNING ELECTRON MICROSCOPY	62
10	COMPRESSIVE TESTING.....	66
	CONCLUSION	70
	REFERENCES.....	72
	LIST OF SYMBOLS	76
	LIST OF FIGURES	78
	LIST OF TABLES	80
	LIST OF APPENDICES	81

INTRODUCTION

The use of polymeric materials is rapidly growing in recent years. They replace common materials such as metals, wood and natural fibers in many applications.

One of the most widely used commercial polymers is isotactic polypropylene (iPP) because it has many desirable and beneficial physical properties such as high melting point, low density, excellent chemical resistance, high tensile modulus and at the end its lower cost.

Nevertheless, the iPP, does not matter, if it is prepared by Ziegler-Natta or metallocene catalysts has a predominantly linear molecular structure and narrow molecular weight distribution. That leads to a variety of melt-processing shortcomings. It exhibits low melt strength and no strain hardening behavior in the melt state, which limits its use in applications such as thermoforming, blow molding, foaming and extrusion coating, where the type of flow is predominantly elongational. As a result, iPP has been limited in some end-use fabrications. Therefore, the preparation and research on high melt strength PP are very active in the past decade [1, 2].

One the most effective method to achieve the high melt strength PP is to introduce long chain branches (LCB) onto PP backbone. The constrain geometry catalyst has been found to be very useful for preparing LCB-PP. However, this method is often used in laboratory. Beside this method there are two other methods, having been applied in industry. One of them is electron beam irradiation which is carried out when PP is in solid state and the second is post-reactor chemical modifications, which is carried out when PP is in melt state [3].

The LCB-PP structure can improve the processing ability of iPP under melt conditions, including strain hardening, shear thinning, high melt strength and so on, thus broadening the end-uses and processing methods of iPP [2]. The commercial LCB-PP, recently developed and introduced in the market by major international polypropylene producers is also called High melt strength polypropylene (HMS-PP).

Because of its special chain structure, LCB-PP is believed to show different helical conformation and crystallite structure in the process of crystallization [2]. It has been reported that LCB-PP crystallizes faster than common iPP, moreover, with higher tendency

to form orthorhombic γ -phase under pressure. This polymorph of iPP processes different physical properties than common monoclinic α -phase [1, 2, 4].

In this context, the purpose of this Master thesis is to analyze crystallization behavior of LCB-PP (Daploy WB130HMS) produced by Borealis Company under increased pressure. High pressure crystallization equipment pvT100 is used for sample preparation. Investigation of prepared samples is carried out using several experimental techniques such as wide angle X-ray scattering, differential scanning calorimetry, scanning electron microscopy and compressive testing.

I. THEORETICAL PART

1 CRYSTALLIZATION OF POLYMERS

Crystallization is the process of formation of solid crystals precipitating from a solution, melt or more rarely deposited directly from a gas. As heat is removed from melt during processing, molecules begin to lose the ability to move freely, and the melt becomes more viscous. Crystallization plays an important role in industrial processing of semi-crystalline resins. It strongly affects rheological properties of polymer melts and solutions, influences mechanical and barrier properties of solid objects [5].

At the crystallization temperature (T_c), molecules begin to arrange themselves into crystals and ordered crystalline regions, along with disordered amorphous regions. The region of crystallization temperature is between the melting temperature of polymer (T_m) and the glass-transition temperature (T_g), whereas the former is always higher than the latter.

Crystallization is generally favored by slower cooling from the melt, very rapid cooling can suppress crystallization. Polymers are never totally crystalline, as a consequence of their long chain nature and subsequent annealing. The crystallinity depends primarily on the regularity (chemical, geometrical and spatial) of the macromolecular chains. The more regular the polymer the more likely it is to crystallize [6].

The crystallization process consists of two major plots, nucleation and crystal growth. Crystals are created when nuclei are formed and then grow. The kinetic processes of nucleation and crystal growth require supersaturation, which can generally be obtained by a change in temperature, by removing the solvent, or by adding a drowning-out agent or reaction partners.

1.1 Nucleation

Nucleation is the extremely localized budding of a distinct thermodynamic phase. The system attempts to achieve thermodynamic equilibrium through nucleation and the growth of nuclei. If a solution contains neither solid foreign particles nor crystals of its own type, nuclei can be formed only by homogeneous nucleation. If foreign particles are present, nucleation is facilitated and the process is known as heterogeneous nucleation. Both homogeneous and heterogeneous nucleation take place in the absence of solution own crystals and are collectively known as primary nucleation. Secondary nucleation results from contact, shearing action, breakage, abrasion and needle fraction. However, it should

be noted that a distinction is made between them [7]. Various kinds of nucleation are shown in *Fig. 1*.

No matter whether nucleation is homogeneous or heterogeneous it is still strongly affected by molecular weight, with longer molecules usually initiating crystallization of the polymer. Presumably this is because the longer a molecule is, the greater the chance of being able to adopt a suitable conformation [6].

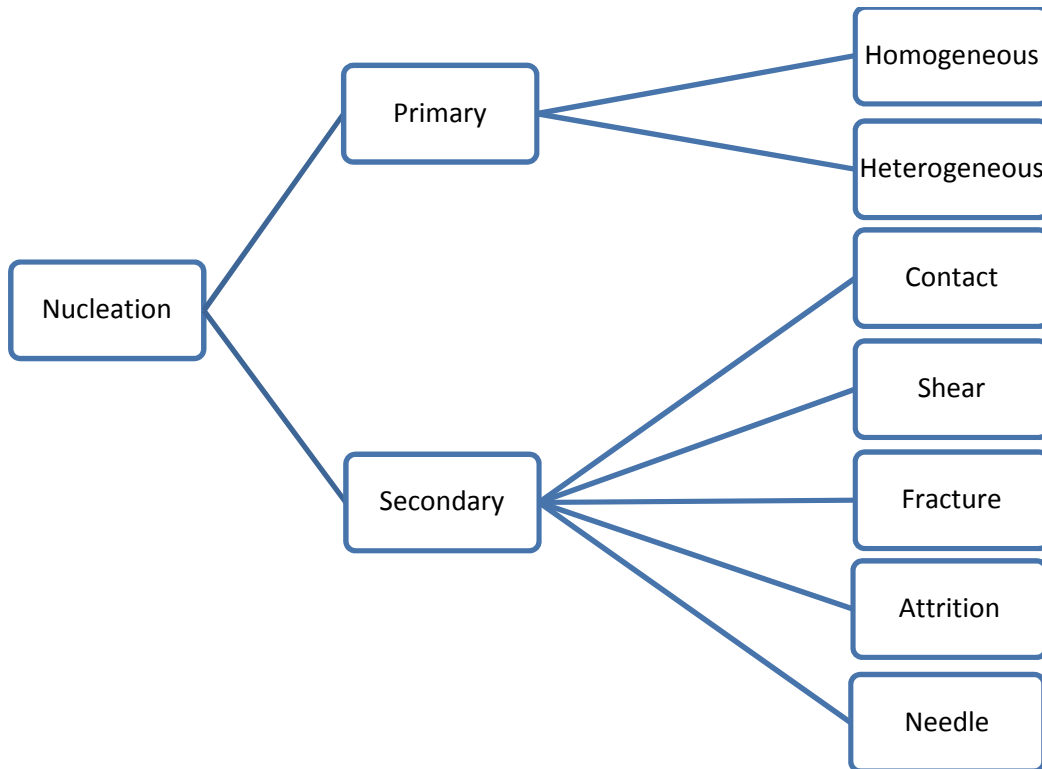


Fig. 1: Various kinds of nucleation

1.2 Crystal growth

Crystal growth is a major stage of a crystallization process, which typically follows an initial stage of either homogeneous or heterogeneous nucleation.

Crystal growth is a diffusion and integration process, modified by the effect of the solid surfaces on which it occurs. Solute molecules or ions reach the growing faces of a crystal by diffusion through the liquid phase. At the surface, they must become organized into the space lattice through an adsorbed layer. Neither the diffusion step nor the interfacial step, however, will proceed unless the solution is supersaturated. The rate of crystal growth can be expressed as the rate of displacement of a given crystal surface in the direction

perpendicular to the face. Different crystallographic faces of a crystal usually have different linear growth rates [8].

In most cases, more than one mechanism influences a crystal's growth rate. If the different mechanism take place in parallel, then the mechanism resulting in the faster growth controls the overall rate. If the processes take place in series, as in the case of bulk infusion followed by surface reaction, then the slower mechanism will control the overall rate [8].

1.3 Morphology of crystalline polymers

The morphology of crystalline polymers (the size, shape and relative magnitude of crystallites) is rather complex and depends on growth conditions such as solvent media, temperature and growth rate. The polymer chains are packed into the unit cell, which is the fundamental element of a crystal structure. Unit cells are geometrical shapes with parallel sides (tetragonal, cubic, hexagonal etc.) that represent the placement of atoms. The atomic arrangement in the unit cell of a polymer is repeated millions of times in three-dimensional space in forming the crystalline structure [9, 10].

1.3.1 Single Lamellae

The helical chains fold back and forth to form thin, ordered, plate-like or ribbon-like structures called lamellae, which are roughly 10 nm thick platelets with regular facets. The thickness depends on crystallization temperature and processing methods. Lamellae are connected by amorphous regions, called "tie points", that result from irregularities in the polymer chain. Tie points provide flexibility and impact resistance to the crystalline regions. A polymer with more tie points is generally stronger. However, too many tie points can result in brittleness, low toughness and low impact resistance. As crystallization proceeds, the growth fronts of two different spherulites meet, and the lamellae extend across spherulite boundaries into uncrystallized material available, which tends to hold the material together. If crystallization occurs rapidly, as it does in crystallization from a melt, the polymer chains can crystallize within more than one lamellae. Interlamellar fibrils tie two or more lamellae together and also bridge spherulite themselves [9, 10].

A schematic representation of a polymer lamellae, based on chain folding model is shown in *Fig. 2*.

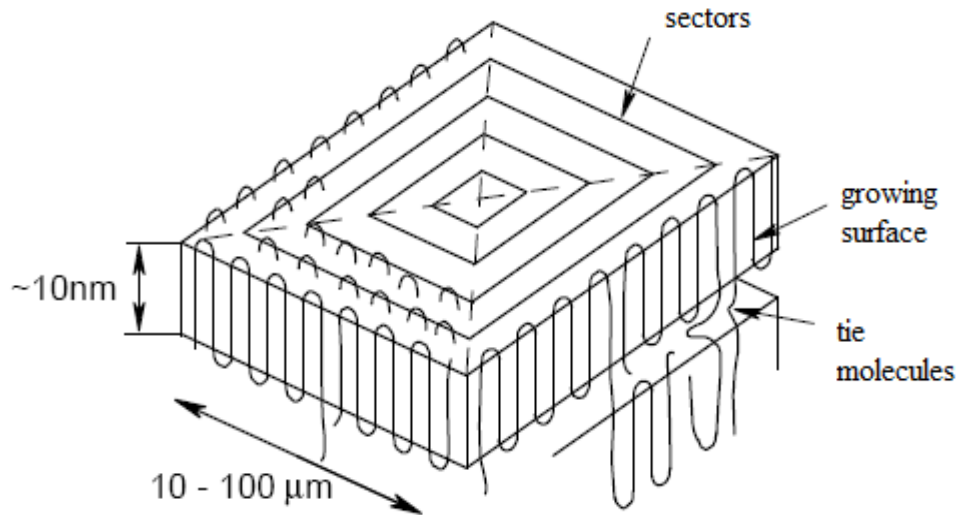


Fig. 2: Polymer single lamellae [11]

1.3.2 Spherulites

The most prominent structural feature of polymers crystallized from the melt is the spherulite. The spherulite is not a single crystal, but an extremely complex spherical aggregate of lamellae ranging in size from about $0.1 \mu\text{m}$ to possibly a few millimeters in diameter. According to a simplified model, crystallites start from a central, pin-point type nucleus and grow uniformly in all spatial directions radially, with noncrystallographic small angle branching in between. The branching of growing crystallites provides complete space filling. Spherulites can be observed with optical microscopy under crossed polarizers as a Maltese cross patterns, as illustrated in *Fig. 3*, arising from the birefringent effects associated with the molecular orientation of lamellae morphology [12].

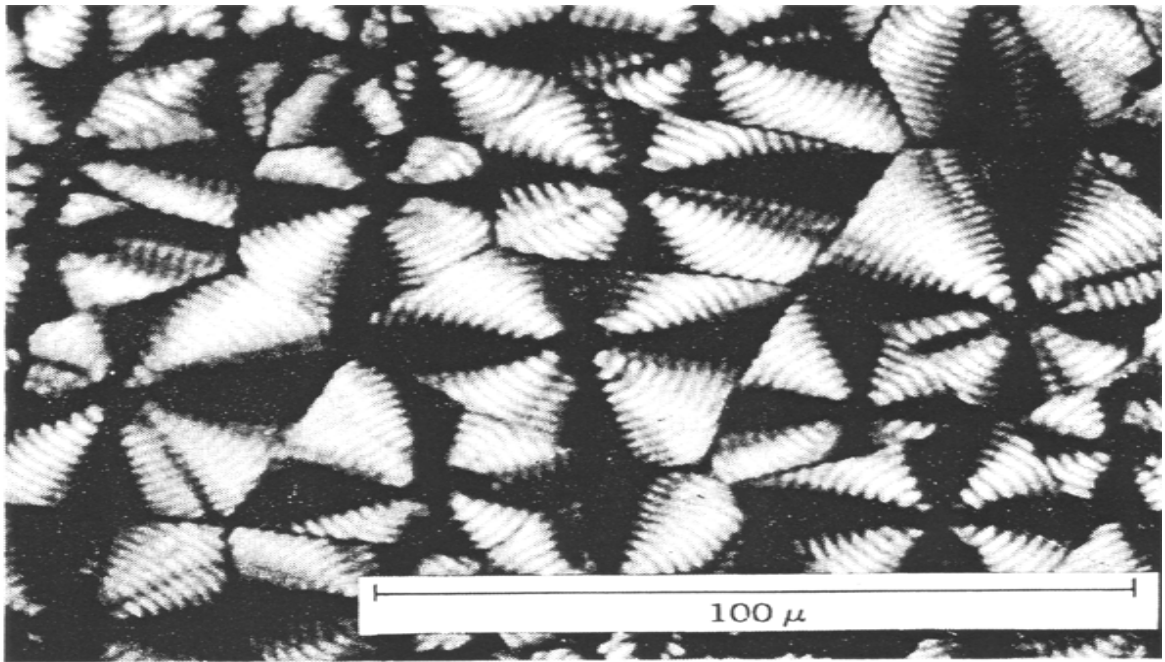


Fig. 3: Maltese cross patterns [13]

The presence of a nucleating agent-provides additional sites for crystal growth, resulting in smaller, more numerous spherulites in the crystallized polymer. Many organic compounds and metal salts can act as nucleating agents, including colorant pigments and residual monomer. When nucleation occurs at about the same time the boundaries of the spherulites appear to be somewhat straight. When nucleation occurs at different times the spherulites are different sizes and the boundaries hyperbolas. Rapid cooling decreases the amount of spherulite formation presumably because of a lack of time to allow the chains to organize into spherulite structures [10, 14].

The growth rate of spherulites is remarkably linear with time at a given temperature, except when the viscosity of the melt is deliberately reduced. The development of spherulites growth is shown in *Fig. 4*.

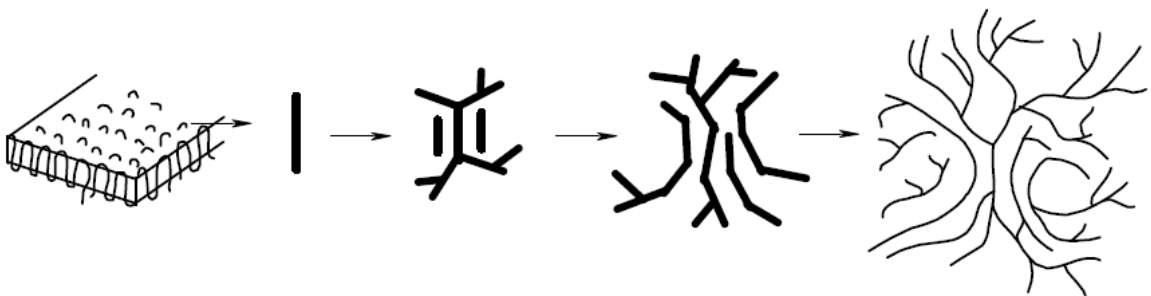


Fig. 4: Schematic development of spherulites growth [11]

1.4 Crystallization under high pressure

So far more studies of pressure effects on the polymer crystallization have been carried out to understand the pressure dependency of morphology, internal structure and phase diagram. There have been some reports on crystallization kinetics under high pressures, and they are generally described by Avrami equation [15].

1.4.1 Avrami equation

The original derivations by Avrami have been simplified by Evans and put into polymer context by Maeres and Hay. In the following, it is helpful to imagine raindrops falling in a puddle. These drops produce expanding circles of waves that intersect and cover surface. The drops may fall sporadically or all at once. In either case they must strike the puddle surface at random points. The expanding circles of waves, of course, are the growth fronts of the spherulites, and the points of impact are the crystalline nuclei.

The familiar form of the Avrami equation:

$$1 - X_t = \exp(-Kt^n) \quad (1)$$

where X_t is the volume fraction of crystalline material, known widely as the degree of crystallinity, K and n are suitable parameters, K is temperature dependent.

Avrami equation is often written in logarithmic form:

$$\ln(1 - X_t) = -Kt^n \quad (2)$$

The equation has been derived for spheres, discs, and rods, representing three-, two-, and one-dimensional forms of growth.

The Avrami equation represents only the initial portions of polymer crystallization correctly. The spherulites grow outward with a constant radial growth rate until their impingement takes place when they stop growth at the intersection. Then a secondary crystallization process is often observed after the initial spherulite growth in the amorphous interstices [16].

1.4.2 Formation of γ -form of iPP

It is well known that iPP can exist in three polymorphic crystalline forms, monoclinic α , trigonal β , and orthorombic γ , that differ in the arrangement and packing of the chains [17]. α -form is the most common crystal form, the metastable β -form is obtained sporadically at high supercoolings or in the presence of selective β -nucleating agents [18]. γ -form originates at special crystallization conditions such as crystallization at elevated pressures of the homopolymer, crystallization at atmospheric pressure of low molecular weight fractions, presence of chain defects or chemical heterogeneity or of presence of the comonomer units in the chain [12]. The individual polymorphs of isotactic polypropylene are described in detail thereafter (chapter 2.3).

When varying the pressure during crystallization both the α - and γ -forms are observed. As the crystallization pressure increases the γ -form coexists with the α -form until it becomes dominant at 200 MPa and above [19, 20].

More recent experimentation has shown that for crystallization at a constant pressure the γ -form is the preferred form at low supercoolings.

The consequence of applying pressure should result in a lower opacity and to promote the extended chain nature of iPP, thus facilitating the crystallization into the γ -form.

2 POLYPROPYLENE

Polypropylene is one of the most often used thermoplastic material, due to its favorable properties and low price. Polypropylene is compatible with many processing techniques and used in a wide variety commercial applications. The worldwide consumption of polypropylene occupies the second place among commodity plastics, after polyethylene [21]. This material was introduced to the large scale production in 1957 [22].

2.1 Polymerization

Polypropylene was first polymerized in 1954 by Giulio Natta who was following the work of Karl Ziegler. 'Ziegler type' catalysts were capable of producing high molecular weight polymers from propylene and many other olefins. The monomer for PP is obtained by the cracking of petroleum products, such as natural gas or light oils. For the preparation of polypropylene the C_3 fraction (propylene and propane) is the basic intermediate and it can be separated from the other gases without undue difficulty by fractional distillation. Polypropylene is then prepared using 'Ziegler type' catalysts or metallocene catalysts by a polymerization. A typical catalyst system may be prepared by reacting titanium trichloride with aluminium triethyl, aluminium tributyl and aluminium diethyl monochloride in naphtha under nitrogen to form slurry consisting of about 10 % catalyst and 90 % naphtha. The properties of the polymer are strongly dependent on the catalyst composition and its particle shape and size [23].

2.2 Chemical structure

Polymerization of non-symmetrical propylene molecule leads to three possible sequences. PP molecules are usually added head to tail which results in a polypropylene chain with pendant methyl groups attached to alternating carbons. Occasionally molecules are added head to head or tail to tail, however this alternating arrangement is disrupted. There are three types of PP according to the position of the methyl group: isotactic, syndiotactic and atactic [10].

2.2.1 Isotactic polypropylene

It is the most common commercial form, pendant methyl groups are all in the same configuration and are on the same side of the polymer chain (see *Fig. 5*). Due its tacticity, iPP is the most stereo-regular structured polypropylene when compared to atactic and syndiotactic polypropylenes and thus higher degree of crystallinity is involved [10].

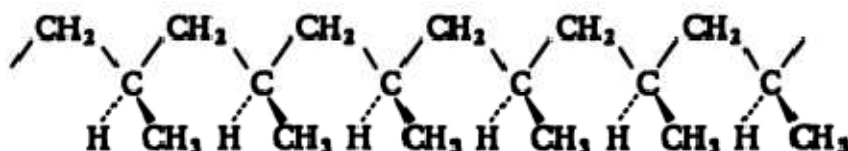


Fig. 5: Isotactic polypropylene [24]

2.2.2 Syndiotactic polypropylene

In syndiotactic polypropylene, alternate pendant methyl groups are on the opposite sides of polymer backbone, with exactly opposite configurations relative to the polymer chains (see *Fig. 6*). Interest in this material is a consequence of its possessing greater toughness, clarity and heat resistance (softening point) than corresponding isotactic polypropylene [10].

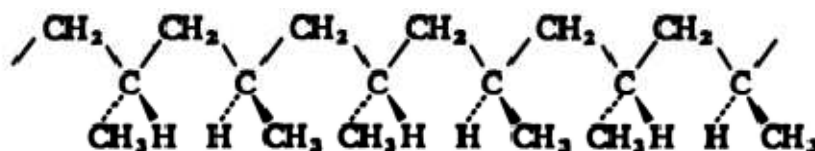


Fig. 6: Syndiotactic polypropylene [24]

2.2.3 Atactic polypropylene

Atactic or amorphous polypropylene is characterized by a random steric orientation of the methyl pendant groups on the tertiary carbon atoms along the molecular chain (see *Fig. 7*). The random sequence of these methyl substituents is linked to an atactic configuration. Generally atactic polymers are characterized by their tacky, amorphous behavior and low molecular weights [12].

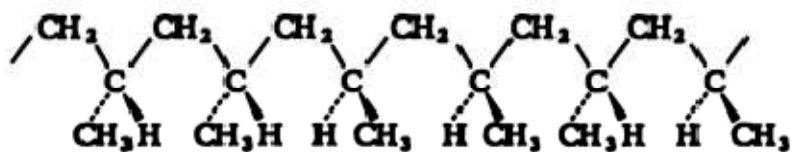


Fig. 7: Atactic polypropylene [24]

Most polymers are predominantly isotactic, with small amounts of atactic polymer. New metallocene catalysts make possible other stereochemical configurations, such as hemiisotactic polypropylene. In this configuration, the most pendants methyl groups are on the same side of the polypropylene chain, as in iPP. However, other methyl groups are inserted at regular intervals on the opposite side of the chain [10].

2.3 Polymorphism of isotactic polypropylene

On the crystal lattice level, isotactic polypropylene exhibits three different morphological forms, depending on the tacticity of the resin and the crystallization conditions, such as pressure, temperature, and cooling rate. Different forms can coexist, and one polymorphic form can change into another as conditions change [10]. The X-ray patterns of three forms (α -form, β -form and γ -form) are shown in Fig. 8.

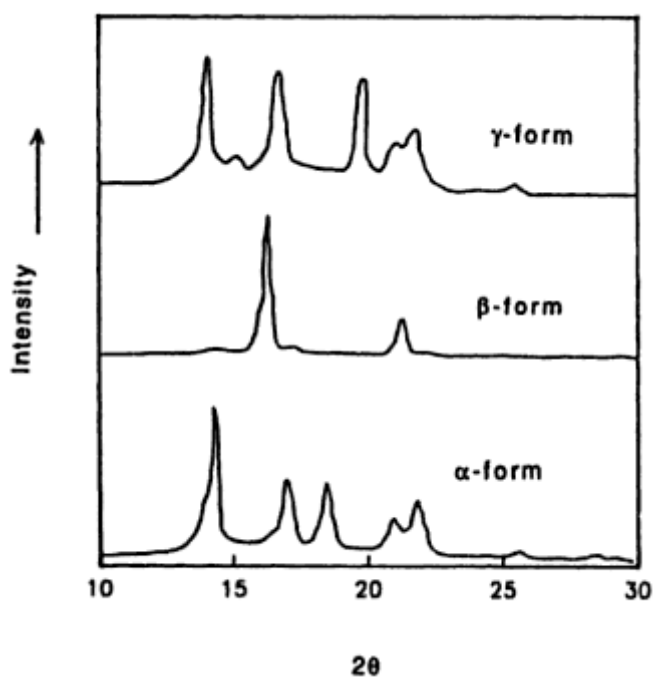


Fig. 8: Unoriented powder WAXD patterns for different forms in iPP crystals [19]

2.3.1 α -form

The predominant and most thermodynamically stable crystalline structure of pure isotactic polypropylene at atmospheric pressure is monoclinic α -form (see Fig. 9). Polymer chains in the α -form of isotactic polypropylene fold into lamellae with thicknesses of 5-20 nm. Radial growth of lamellae is dominant, however, lamella can also associate tangentially, with the tangential lamella branching off approximately orthogonally from the plane of the radial lamellae. This forms a cross-hatched structure in the lamellae, which aggregate to form spherulites [23].

The lamellar structure produces positive, negative, and mixed birefringence. Negative birefringence results from spherulites in which radial lamella are dominant, while positive birefringence is due to spherulites with predominantly tangential lamellae. Both negatively and positively birefringent spherulites form a Maltese cross pattern under crossed polarizers. In spherulites with mixed birefringence, neither tangential nor radial lamellae are predominant, and a distinct Maltese cross is not formed. The birefringence changes from positive to negative with increasing crystallization temperature, as the tangential lamella undergo premelting. The α -form of isotactic polypropylene is the primary phase of polypropylene obtained under usual processing conditions [10].

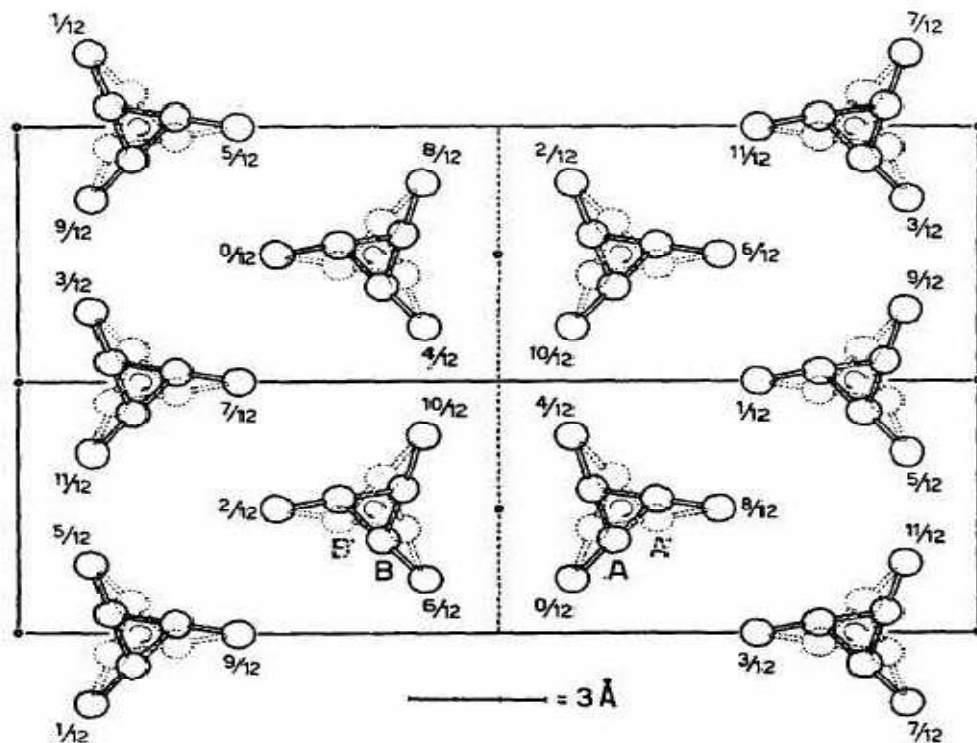


Fig. 9: Crystal structure of α -form of iPP [12]

2.3.2 β -form

The β -form of iPP was firstly identified in 1959 by Keith et al. In the crystallization of conventional iPP grades, a small amount of β -form occurs sporadically at high supercoolings ($T_c < 130$ °C) or in quenched samples [12].

The β -form of isotactic polypropylene has been described to have hexagonal unit cell structure, with more disorder than the α -form. However, Varga and some other authors have recognized β -form to have the trigonal unit cell (see *Fig. 10*) [12].

The parallel, stacked lamella do not show cross-hatching. Lamella have been observed to form sheaf-like spherulitic structures with interconnected boundaries, different from the distinct boundaries of α -form spherulites; in experiments with high purity β -form polypropylene, this structure resulted in lower elastic moduli and yield strength at a given strain rate and higher impact strength and breaking strain values than α -form polypropylene. The β -form exhibits negative birefringence under crossed polarizers and can convert to the α -form on heating. Polypropylene can crystallize in the β -form at relatively low isothermal crystallization temperatures or in the presence of nucleating agents, such as the combination of pimelic acid and calcium stearate [10].

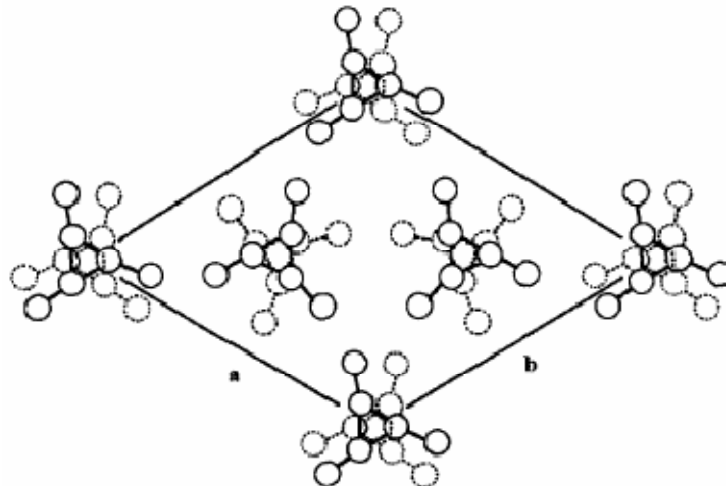


Fig. 10: Crystal structure of β -form of iPP [12]

It was found, that iPP rich in β -form embodies improvement of some mechanical properties. In particular the impact strength, toughness and whitening under tensile deformation of β -iPP (iPP with predominant β -form within the crystalline portion)

markedly exceed those of polypropylene with predominant α -form. However, the presence of β -form in the material decreases stiffness and E-modulus [18, 25, 26].

2.3.3 γ -form

This form was discovered in 1961 by Addick and Beintema. It was produced by crystallization at elevated pressures from high molecular weight homopolymer. The γ -form predominates when the pressure during the crystallization is higher than 200 MPa. Other procedure which leads to the growth of this form is crystallization from melt of high molecular weight stereoblock copolymer with small amounts of ethylene or but-1-ene [27].

The γ -form of isotactic polypropylene was initially considered to have a triclinic unit cell with dimensions similar to α -form, but the crystal structure was recently reassigned as an orthorhombic unit cell with nonparallel, crossed lamellae (see *Fig. 11*). In experiments with polypropylene crystallized at high pressures and different crystallization temperatures, the crossed lamellae formed a feather-like structure, which result from self-epitaxial (tangential) growth [10].

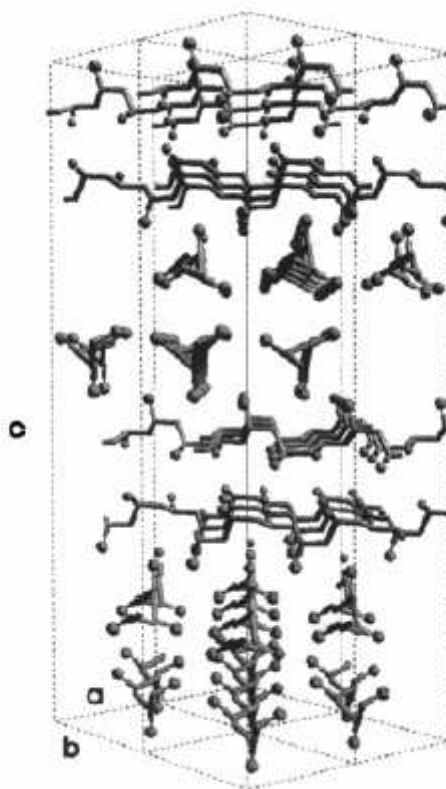


Fig. 11: Four unit cells of the γ -form of iPP according to the nonparallel chain packing model of Meille et al. [28]

On the spherulitic level, pure γ -form shows negative birefringence, lathlike structure of the α -form is absent in the γ -spherulites. The melting point of the γ -form is mostly reported in the range of 125 to 150 °C for low molecular weight samples. In the case of pressure crystallized samples of high molecular weight iPP, the melting point occurs above 150 °C [27].

2.4 Properties and applications of polypropylene

Mechanical properties strongly depend on its crystallinity. Increasing crystallinity enhances stiffness, flexural strength and yield stress, however, decreases toughness and impact strength [10].

Comparison of properties of all stereo-isomers of polypropylene is given in *Tab. 1* [29].

Tab. 1: Properties of isotactic PP, syndiotactic PP and atactic PP [29]

Property	Isotactic PP	Syndiotactic PP	Atactic PP
Density [$\text{kg}\cdot\text{m}^{-3}$]	920–940	800–910	850-900
Melting temperature [°C]	165	135	-
Solubility in hydrocarbons [20 °C]	no	middle	high
Yield strength	high	middle	very low

Polypropylene is used for wide scale of products, such as automotive industry, household goods, domestic appliances, pipes and fittings, furniture, films are used in packaging applications and important application are fibres.

2.5 Long chain branched polypropylene

In the past decade, many researchers have investigated long chain branched (LCB) polyolefin by rheological method, but most studies focus on polyethylene (PE) or model polymers, and only a few literatures are about long chain branched polypropylene (LCB-PP), because LCB-PP is difficult to be obtained and the degree of LCB is very low. When PP is modified by peroxide and polyfunctional monomer, the reaction and the product

components become very complex. Degradation reaction makes the molecular weight to decrease, grafting reaction introduces short chain branch (SCB) structure, branching reaction introduces LCB structure, and gel will be produced if crosslinking reaction can happen. The complex reactions as well as the complex products make the investigation on LCB very difficult [2].

There is no specific definition about LCB, however, from rheological viewpoint, the length necessary for a branch to behave as a long chain branch is $2 Me$ (Me = molecular weight between entanglements). Therefore, the molecular architectures for grafted PP and LCB-PP are very different. As a result, crystallization behavior and crystal morphology of LCB-PP will be different from linear PP or grafted PP [1].

2.5.1 Polymerization

Since long chain branching is generally known to enhance the melt properties of a polymer, several approaches have been developed to make branched polypropylenes. Some include post-reactor treatments such as electron beam irradiation, peroxide curing, and grafting; others use in-reactor copolymerization. The branches in irradiated or peroxide treated polymers are generated through radical-induced random chain scission followed by recombination. Thus, the products are complex, and the processes may be difficult to control. Grafting of polymer chains onto linear macromolecules would lead to comblike branched polymers, but the chemistry to prepare polyolefin graft copolymer is very limited [30].

Polymerization using heterogeneous catalysts

Through the utilization of metallocene catalyst technology, many structures features, including long chain branching, can be introduced into polymer chains during polymerization.

The unique procedure to synthesize LCB-PP via the metallocene mediated polymerization of propylene with T-reagent is called one-pot polymerization process. This procedure allowed for the formation of trifunctional branch points with a relatively well-defined LCB structure. The reaction mechanism of forming LCB-PP polymers via metallocene-mediated propylene polymerization, using isospecific $rac\text{-}Me_2Si[2\text{-}Me\text{-}4(1\text{-}NaPh)Ind]_2ZrCl_2/MAO$ catalyst, in the presence of T-reagent, p-(3-butenyl) styrene (BSt) that serves as both comonomer and chain transfer agent.

Basically, branches in LCB-PP can be formed when a growing polymer chain either incorporates the but-3-ene chain-end of a macromonomer or chain transfers to the pendant styrene of a copolymer (*Fig. 12*). The pre-dominant route for the formation of branches involves the pendant styrene of the copolymer, which serves as the chain transfer agent to form the LCB-PP in the presence of hydrogen. The presence of hydrogen can relieve the dormant catalyst site via a subsequent chain-transfer reaction to produce a macromonomer with the α -olefin but-3-ene at the chain-end [31].

The values like molecular weight (M_w) branching degree and melt flow rate (MFR) are achieved by controlling the reaction conditions.

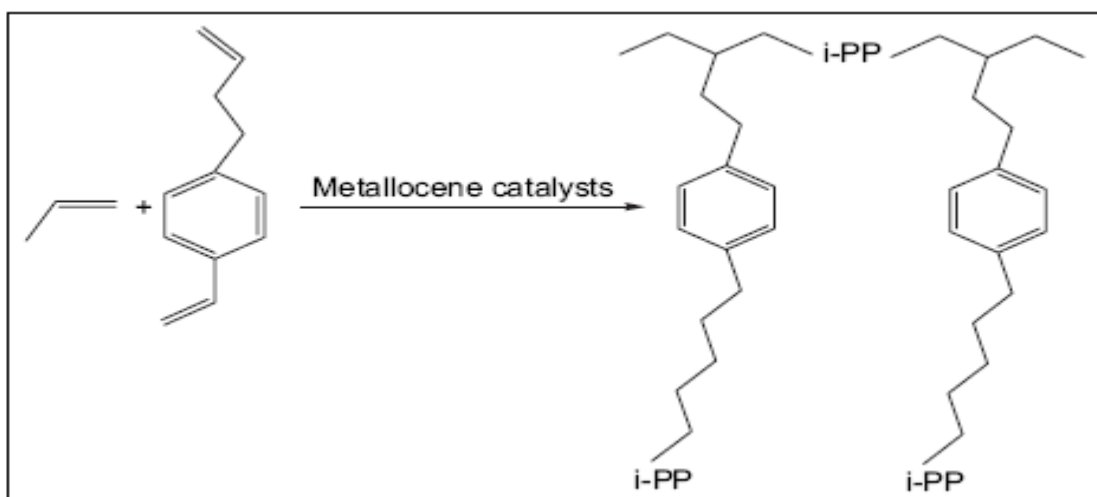


Fig. 12: Preparation of LCP-PP by using heterogeneous catalysts [2]

Polymerization by radical reactions

There are two methods of radical modifications. The first is electron beam irradiation which is a physical method and it generates modification effects in the macromolecular structure and material properties. The second one is chemical method which contains modification of PP with peroxides in combination with multifunctional monomers or the reactive extrusion of PP with peroxydicarbonates (PODIC).

Two mechanisms of radical reactions (in inert atmosphere and in the presence of monomer) are shown in *Figs. 13* and *14*.

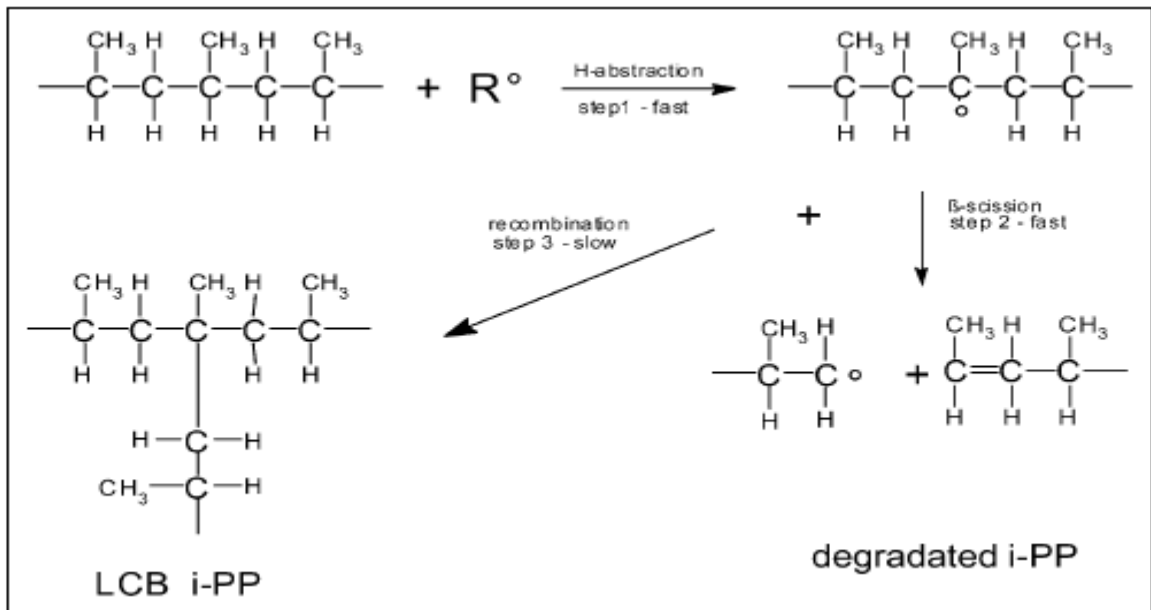


Fig. 13: LCB-PP by radical reaction in iPP below 80 °C in inert atmosphere [32]

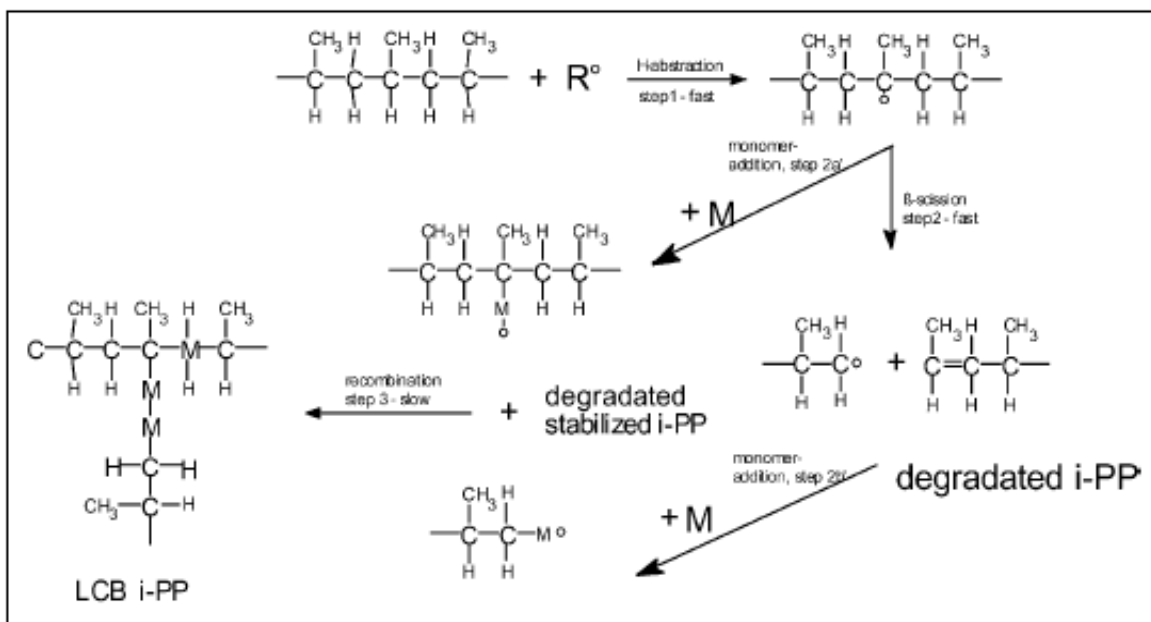


Fig. 14: LCB-PP by radical reaction on iPP at higher temperatures in presence of monomer [32]

Polymerization by ionizing radiation

The radiation process has played an important role to produce polymers with these controlled rheological properties. The irradiation of polymeric materials with ionizing radiation (accelerated electrons, X-rays, ion beams, gamma rays) creates very energetic ions and excited states, which decay to reactive free radicals. These intermediate species can follow several reaction paths, resulting in the new bonds formation (see *Fig. 15*), as well as in the case of peroxide degradation process. The degree of transformation depends on the structure of the polymer and the conditions of pre-treatment, during and after irradiation as well as dose rate [33].

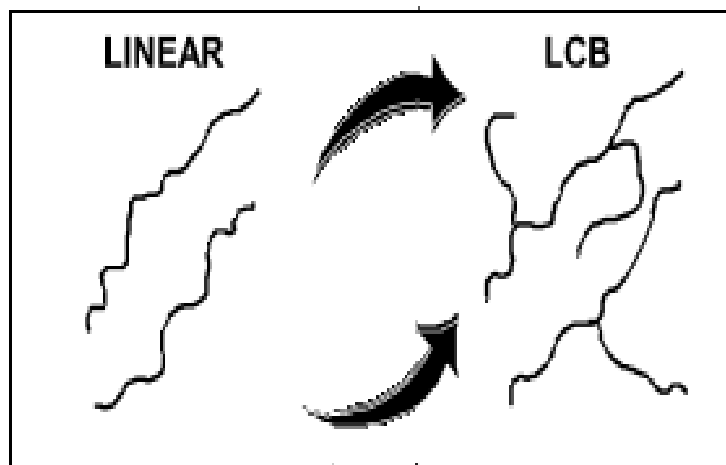


Fig. 15: Conversion of the linear iPP structure into a LCB material [32]

Irradiation processing is mostly realized in the polymer solid state, however, the electron beam irradiation of PP in the molten state is an additional way of creating LCB without additives.

The formation of chain branching or crosslinking is located mainly in the amorphous regions. The material in the molten state contains no crystalline regions. This leads to the conclusion that all chains are available for branching reactions. Therefore, the chance of chain branching during irradiation in the molten state of the material is much higher than in the solid state. In the solid state, the branching reactions are limited by the diffusion of chain fragments. Moreover, the thermal degradation of the molecular weight at high temperatures is enhanced [34].

Polymerization using peroxides

The next way to produce LCB-PP is by reactive extrusion in the presence of peroxydicarbonate (PODIC), shown in *Fig. 16*. The amount of LCB can be controlled by the type and the amount of PODIC used for the modification. A perester with the same reactivity shows an opposite behavior inducing degradation through β -scission and leading to lower extensional viscosity without strain hardening, lower melt strength, lower die swell and higher MFI [35].

The peroxide structure has a direct influence on the branching level of modified PPs. PP has a tendency to undergo β -scission because of the nature of its molecular structure, and this competes with grafting and cross-linking reactions during the reactive extrusion process. The use of polyfunctional monomers can decrease the degradation and improve the degree of branching for PP [35].

PODIC with long linear alkyl groups are more efficient in adding branches to PP than the ones with shorter groups. Non-linear alkyl groups result in samples with more branches and strain hardening than the ones with linear groups and comparable number of carbon atoms [35].

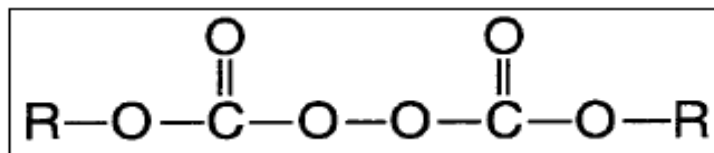


Fig. 16: General formula of PODIC [35]

2.5.2 Crystallization

Because of its special chain structure, LCB-PP is believed to show different helical conformation and crystallization structure in the process of crystallization. The different helical conformation and complicated crystallization structure will greatly influence the processing ability of LCB-PP [2].

The change of molecular architecture can affect not only rheological property but also crystallization property of PP. There have been many studies on the crystallization of grafted PP, as a consequence is widely accepted that the branches have the role of

heterogeneous nucleating agent for the matrix and accelerates the crystallization process [4].

Crystallization of the LCB-PP during the fast cooling process, or at lower crystallization temperature, leads to the formation of mainly edge-on lamellar structure. Crystallizing LCB-PP at moderate temperature range results in the formation of both edge-on and flat-on LCB-PP crystals, which coexist side by side even in the same spherulite [4].

Both α - and γ - forms develop in LCB-iPP by crystallizing from the melt, among which the γ -form is a metastable crystal with a large amount of structural defects. The γ -form melts at a lower temperature and in a broader temperature range, while the crystals of α -form are instead, probably more perfect and melt at higher temperatures and in a narrower temperature range. The crystallization of γ -form is favored by the presence of the LCB in iPP [2].

The LCB-PP crystals grow, however, slower than their linear counterparts and spherulites are much smaller than that of linear PP, indicating that LCB structure acts as nucleating agent.

LCB-PP has higher crystallization temperature, shorter crystallization time, and broader melting range when compared with linear PP.

2.5.3 Properties

In the past decade there has been an increasing request from market for high melt strength polypropylenes. The melt strength is defined as the resistance of a melt to draw-down and is an important parameter describing the extensibility of a polymer melt which is of great importance in all processing technologies where elongational flows and stretching of polymer melt occur.

It is known that relatively low melt strength and non-strain hardening behaviour of the linear polypropylene limit its use in application such as thermoforming, foaming and blow molding. One of the most effective approaches to achieve high melt strength for PP is to introduce long chain branches onto PP backbone. Long branched chains increase the chain entanglement level, thereby increasing melt strength as well as the final mechanical properties of the materials, e.g., higher flexural modulus and tensile yield strength. The melt strength also increases strongly with decreasing melt flow index (MFI), as well as by widening the molecular weight distribution. On the other hand, branched polypropylenes

obtained using electron beam irradiation were found to have ten times higher melt strength than a linear PP with the same MFI. It is expected that if the melt strength behaviour of PP is improved, its market position will become even more prominent, replacing other thermoplastics in several applications [36, 37]. The comparison of some physical properties of LCB-PP and linear PP is listed in *Tab. 2*.

Tab. 2: Mechanical properties of modified polypropylene material with long chain branches compared to linear polypropylene with identical melt flow rate [36]

Property	Unit	Branched material (Daploy HMS)	Linear PP
Tensile modulus	MPa	2 000	1 500
Tensile strength at yield	MPa	40	33
Heat deflection temperature	°C	60	56
Charpy impact strength, notched (23 °C)	kJ/m ²	3	4
Charpy impact strength, notched (-20 °C)	kJ/m ²	1	11

The stiffness of polypropylene is increased and impact strength remains unchanged if polypropylene is used as starting material for solid phase modification. This improvement is caused by a self nucleation by long chain branches of molecules having an extremely high molecular weight in branched part [32, 35].

2.5.4 Application

Foam extrusion

It has been realized for a number of years that in order to produce high quality PP foam, high melt strength PP (HMS-PP) is required; however, PP foams are relatively late comer to this market. PP induces a lot of problems during the process, the reason lies in the molecular structure. Standard PP's lack the required extensional rheological properties in the melt phase which are required for the production of extruded low density foams with a fine and controlled cell structure. The availability of HMS-PP (i.e. LCB-PP), the above mentioned problems are reduced or even solved. These HMS-PP resins offer property

benefits such as a wide mechanical property range, high heat stability, good chemical resistance and no monomer issues, and in the melt phase it is high strength and high drawability. Outstanding properties of all foams based on HMS-PP are the possible weight reduction, material savings, and good environmental credentials [32, 38].

The global PP foam market is growing rapidly, current HMS-PP foam applications are:

- thermo-formable technical foams for automotive applications;
- lightweight packaging trays, beakers and containers for food packaging;
- thermo-formable foamed films, sheets and planks;
- microwaveable containers for heating of food stuff.

Film blowing

The use of PP in blown film technology was limited by its low melt strength, which is leading to low bubble stability, low output, wrinkles on the reel, inhomogeneous thickness distribution on the product size and non-economic operation on processing side.

The addition of long branches decreases the haze value for the films; this could be of interest for applications where film transparency is an important issue [39].

HMS-PP can significantly improve the processing and the resulting film quality. By stabilizing the bubble and reducing the wrinkling at the reel, process stability and output can be increased [32].

Potential applications are:

- easy tear packaging;
- hygienic films, e.g. diaper films.

Thermoforming

In recent years thermoforming of polypropylene has made massive progress in applications ranging from food packaging to large industrial parts, despite that it is difficult to thermoform polypropylene. This progress could only be made by designing specialized thermoforming technique and equipment on the one hand and innovative polypropylene resin developments on the other hand.

The thermoforming of polypropylene can be significantly improved by the addition of long chain branches to standard polypropylene [32].

3 METHODS OF ANALYSIS

3.1 Wide angle X-ray scattering

Wide angle X-ray scattering (WAXS) is the most commonly used technique for obtaining information about the size and shape of crystallites, and about the degree of crystallinity in solid polymers. WAXS measures the spacing between the ordered crystalline layers (*Fig. 17*) [40]. Bragg derived his now famous equation for the distance d between successive identical planes of atoms in the crystal and λ is the X-ray wavelength:

$$d = \frac{n\lambda}{2\sin\theta} \quad (3)$$

The principle is diffraction of the X-ray radiation beams on the regular structure consequently on the crystal lattice. The crystal diffracts an X-ray beam passing through it to produce beams at specific angles depending on the X-ray wavelength (about 10 nm), the crystal orientation and the structure of the crystal [40].

The intensity of the diffracted X-ray is measured as a function of the diffraction angle 2θ and the specimen's orientation. This diffraction pattern is used to identify the specimen's crystalline phases and to measure its structural properties. WAXS is non-destructive and does not require elaborate sample preparation which partly explains the wide usage of this technique in materials characterization [41].

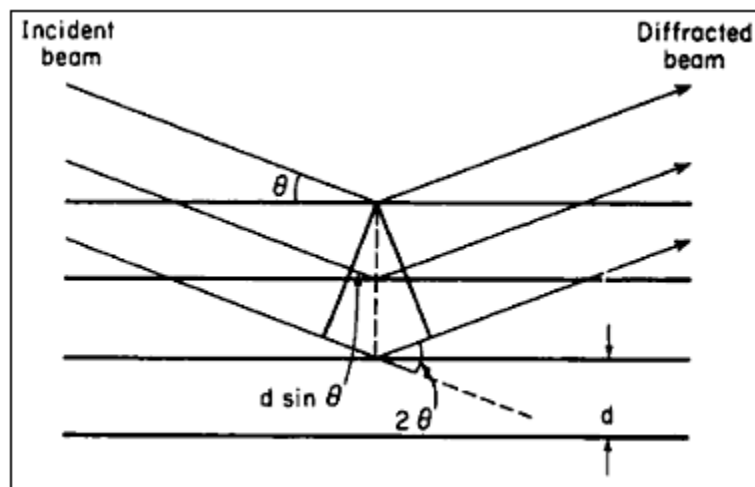


Fig. 17: The Bragg diffracting condition. Difference in path length between successive rays is $2d \sin \theta$ [42]

Crystalline regions show coherent scattering patterns and a sharp peak can be observed in the diffraction versus intensity curve whereas an amorphous phase gives a broad peak. The degree of crystallinity can be obtained by measuring the area under each peak. However, it is often difficult to discriminate between crystalline and amorphous scattering which implies that the degree of crystallinity cannot be determined very accurately. Also the presence of small crystallites is difficult to characterize, because they exhibit similar scattering effects as the amorphous material. However, small crystallites tend to broaden the peaks and sometime information about crystal size can be obtained from such broadening [43].

3.2 Scanning electron microscopy

Scanning electron microscopy (SEM) is the main technique for direct surface investigations. The principle of SEM differs substantially from transmission electron microscopy (TEM). A focused electron beam with accelerating voltage from 0.1 to 50 kV is scanned line by line across the specimen surface. At the incident point of the primary electron beam, secondary electrons are emitted, besides several other electron beam–specimen interactions. The intensity of secondary electrons depends on surface topography, i.e. on the angle between the direction of the primary electron beam and the surface. The number of the secondary electrons modulates the brightness of a display screen, which is controlled by the same scan generator as the primary electron beam. For example, areas with a higher intensity of secondary electrons appear brighter on the display screen than others. This yields a good contrast of SEM images with a very good spatial visibility of details and a high depth of focus (a factor of about 100 greater than in light-optical imaging) [44]. The schematic diagram of scanning electron microscope is shown in *Fig. 18*.

The magnification is attained from the ratio of the size of the display screen to the size of the scanned surface region on the sample, and it can be changed easily between about 5 to 200 000. Therefore, the resolving power of SEM lies between light optical microscopy and TEM [44].

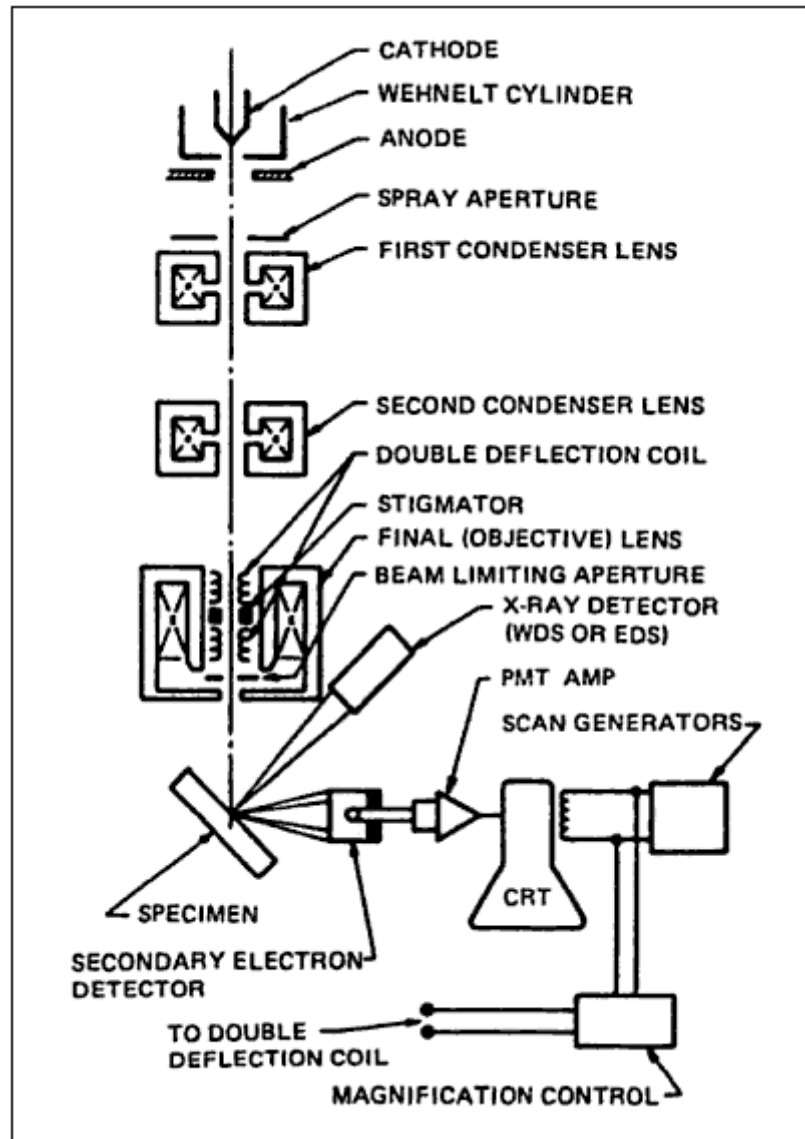


Fig. 18: Schematic diagram of scanning electron microscope [45]

There is a constitutional advantage of SEM that, in general, no special preparations are necessary to perform morphological investigations of specimens [44].

3.3 Differential scanning calorimetry

Differential scanning calorimetry (DSC) is most often used by polymer analysts for determining a polymer's melting temperature, glass transition temperature (T_g), degree of crystallinity, heat of fusion or degree of cure. It is an excellent technique for investigating the failure of polymers owing to the small sample size required, its ability to reveal the

polymer's thermal history, and its ability to measure the T_g of the polymer (which is sensitive to annealing and physical ageing) [45].

Although DSC has become a routine method for polymer analysis, the analyst needs to be aware of possible artifacts that can distort the results. Careful interpretation of thermo-analytical data can be providing a wealth of information for polymer characterization. It is well known that the first heating curve is significantly influenced by the sample's thermal history. It is often useful therefore to compare the first and second heating scans of a polymer sample. Information that can be obtained by this comparison can be related to the thermal history (mould temperature annealing, etc.), crystallinity and recrystallization. It should be noted that, generally, DSC does not detect thermal transitions of minor components in a polymer sample, such as those in a blend (i.e. components that are present at levels less than 5%) [45].

Fig. 19 which illustrates typical polymer thermogram presents some information that can be obtained by DSC analysis.

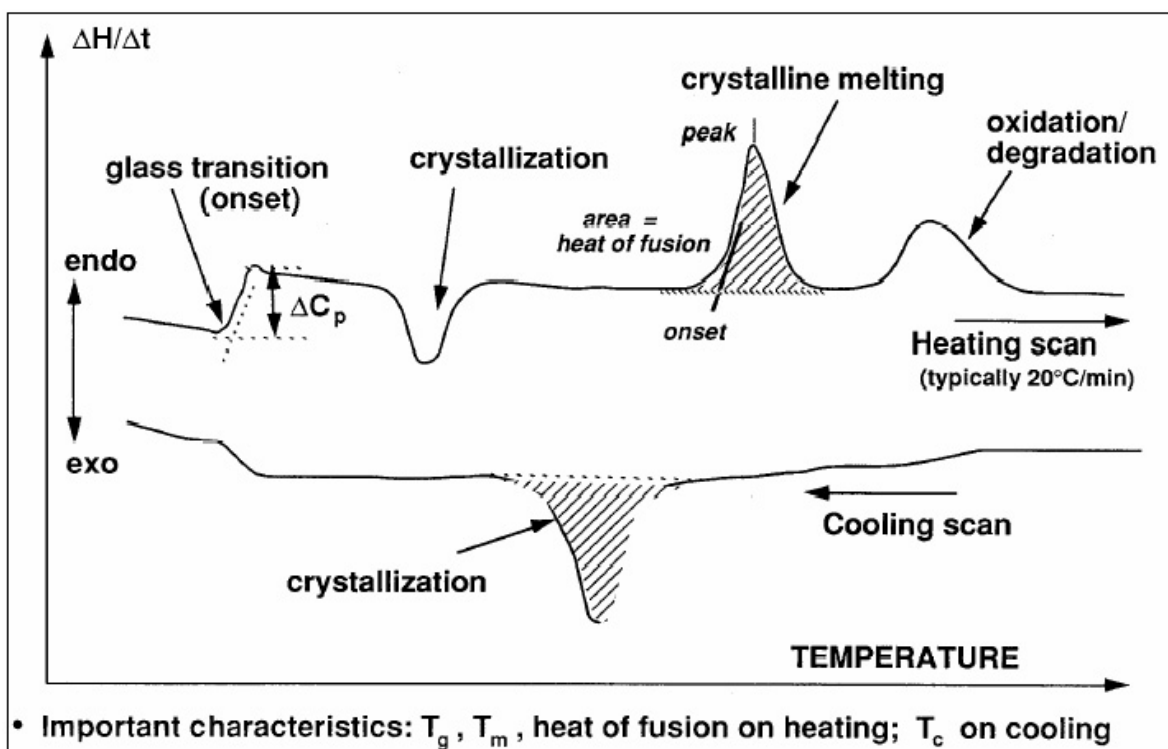


Fig. 19: Typical polymer DSC thermogram [46]

In a cell designed for quantitative DSC measurements, two separate sealed pans, one containing the material of interest and the other containing an appropriate reference, are heated (or cooled) uniformly (see Fig. 20). The DSC cell uses a constantan disk as the primary means of transferring heat to the sample and reference holders and also as one element of the temperature-sensing thermoelectric junction. Samples in powder, sheet, film, fiber, crystal, or liquid form are placed in disposable aluminum sample pans of high thermal conductivity and weighed on a microbalance. The sample is placed in one sample holder and empty sample holder serves as reference. Sample sizes range from 0.1 to 100.0 mg [47].

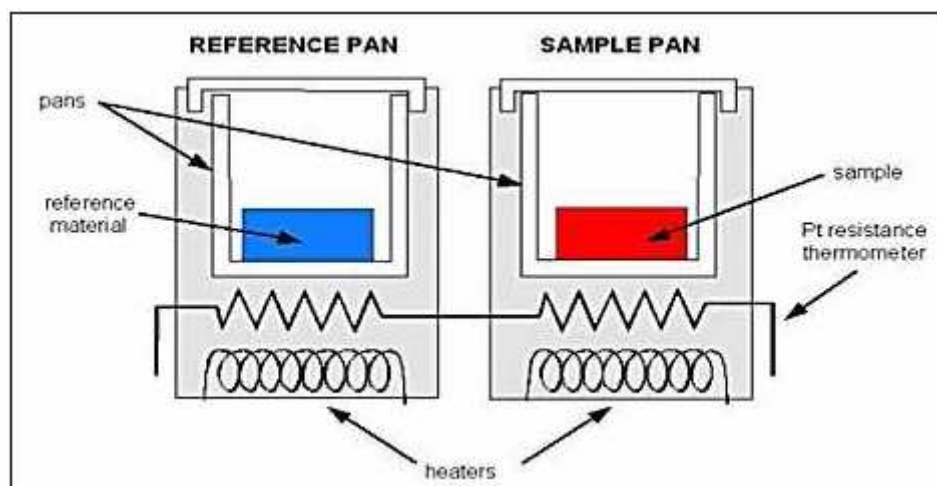


Fig. 20: Schematic diagram of differential scanning calorimetry [48]

3.4 Determination of compressive properties (ČSN EN ISO 604)

Measurements using a single-stage short-range load are the most widely used basic measurements of the mechanical properties of polymers. Technical measurements leading to plotting of stress-strain diagrams are made not only in tension, but also in compression. The stress-strain diagram in compression is used to determine the following parameters: the maximum compressive stress, the ultimate stress in compression, the yield point in compression, modulus of elasticity, the proportional limits, and the secant modulus [49].

The stress in a compression test, as a rule, is determined as the ratio of the load to the original cross-sectional area of the specimen. Deformations in compression are evaluated either according to the reduction in the length of the specimen. The requirement of

improved accuracy of deformation measurement in compression is complied with by increasing the height of a specimen. But this leads to a contradiction with the requirement of specimen stability. Compression tests of standard specimens are usually run at a speed 1 to 20 mm/min. For specimens of other sizes, the speed is found by the formula:

$$v = 0.03h \quad (4)$$

where v is the speed of approach of the plates, and h is the original height of the specimen [49].

In comparison with tension, compression tests have their advantages and their specific difficulties.

The advantages include the use of small specimens and large loads that are easier to measure, and the possibility of methodologically eliminating measurement errors and errors in the deformations associated with the fastening of the specimen in the grips. The shortcomings include by the loss of stability of a specimen, the high requirements to the central application of the load, and to the parallelity of the plates and supporting surfaces of the specimen [49].

II. EXPERIMENTAL PART

4 MATERIALS AND SAMPLE PREPARATION

Throughout this study, three commercially available types of polypropylene were examined.

The first material was long chain branched polypropylene Daploy WB130HMS, which is supplied by Borealis Company, Vienna, Austria. It is a propylene-based, structurally isomeric polymer and was produced by monomer grafting during the radical-driven reactions of isotactic polypropylene with peroxides to create long-chain branches. This material is optimized to deliver improved processability, high stiffness, high service temperature, foamability in foam extrusion processes and good insulation properties of foamed materials. The applications of this material are thermoformable, foamed films and sheets, lightweight packaging trays, microwaveable food packaging, technical foams for automotive applications such as headliners or carpet backing, door liners, parcel shelves, water shields, thermal and acoustic insulation, etc. Physical properties of this material are shown in *Tab. 3*.

Tab. 3: Physical properties of LCB-PP Daploy WB130HMS

Property	Typical Value	Test Method
Melt Flow Rate (230 °C, 2.16 kg)	2.0 g/10 min	ISO 1133
Flexural Modulus (5mm/min)	1 900 MPa	ISO 178
Tensile Modulus (1mm/min)	2 000 MPa	ISO 527-2
Tensile Strength	40 MPa	ISO 527-2
Heat Deflection Temperature A	60 °C	ISO 75-2
Charpy Impact Strength, notched (23 °C)	3.0 kJ/m ²	ISO 179/1eA

The second material examined in this study was polypropylene homopolymer HC600TF. Material is supplied by Borealis Company and is intended for thermoformed packaging applications. It has very good organoleptic properties allowing this grade to be used with any masterbatch without discoloring problems. This material is optimized to deliver very good contact clarity, stiffness, impact balance, processability and melt stability. The applications are in-line and off-line thermoforming, housewares and thin wall packaging,

margarine tubs and it is possible to mix it with copolymer. Physical properties of this material are shown in *Tab. 4*.

Tab. 4: Physical properties of PP homopolymer HC600TF

Property	Typical Value	Test Method
Melt Flow Rate (230 °C, 2.16 kg)	2.8 g/10 min	ISO 1133
Flexural Modulus (5mm/min)	1 500 MPa	ISO 178
Tensile Modulus (1mm/min)	1 600 MPa	ISO 527-2
Tensile Stress at Yield (50mm/min)	35 MPa	ISO 527-2
Heat Deflection Temperature A	85 °C	ISO 75-2
Charpy Impact Strength, notched (23 °C)	4.0 kJ/m ²	ISO 179/1eA

For comparison, also polypropylene homopolymer Borclean HC300BF was examined, what is supplied by Borealis Company. It is a high crystallinity homopolymer film resin. This material has super high purity, contains no slip, antiblock, antistatic additives or nucleating additives. These properties lead to improved high thermal stability, low dissipation factor, good stiffness, outstanding processability, metallisable and very low ash content. This material has been developed especially for applications like dielectrical film for capacitors and metallisable film. Physical properties of this material are shown in *Tab. 5*.

Tab. 5: Physical properties of PP homopolymer Borclean HB300BF

Property	Typical Value	Test Method
Melt Flow Rate (230 °C, 2.16 kg)	2.8 g/10 min	ISO 1133
Flexural Modulus (5mm/min)	1 500 MPa	ISO 178
Tensile Modulus (1mm/min)	1 600 MPa	ISO 527-2
Tensile Stress at Yield (50mm/min)	35 MPa	ISO 527-2
Heat Deflection Temperature A	85 °C	ISO 75-2
Charpy Impact Strength, notched (23 °C)	4.0 kJ/m ²	ISO 179/1eA

In following text, the materials are signed: long chain branched PP Daploy WB130HMS as LCB-PP, homopolymer HC600TF as PP and homopolymer Borclean HB300BF as c-PP (PP clean).

Samples of all used materials were prepared using a pressure-volume-temperature (pvT) technique (i.e. high pressure crystallization).

The produced pellets of each material of weight of approx. 0.7 g were put into a measurement cylinder and heated at the temperature 220 °C with heating rate 80 °C/min. Then, the controlled crystallization from 220 to 50 °C with cooling rate 5 °C/min proceeds samples at several elevated pressures, namely 20, 40, 80, 120, and 160 MPa. The end of crystallization was signaled by the piston holding the same position for 5 minutes. The crystallization process was monitored by computer, which records temperature, time and piston position. The resulting samples (cylinder shape) were prepared with a pvT100 apparatus manufactured by SWO Polymertechnik GmbH (Krefeld, Germany). An instrument for determining the pvT behaviour is shown in *Fig. 21*.

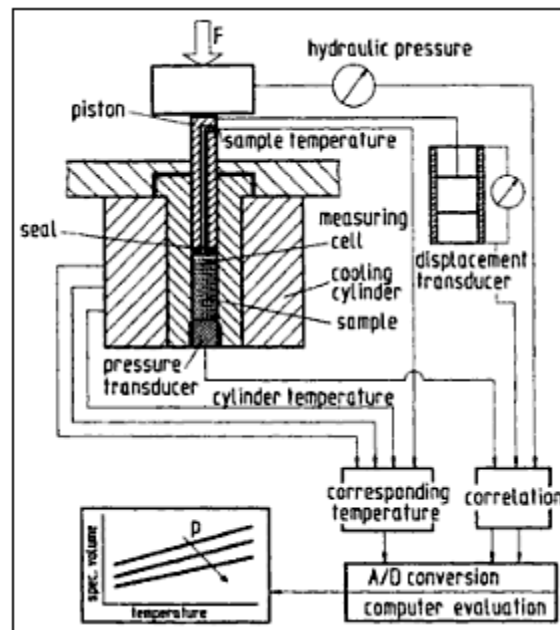


Fig. 21: Instrument for the measurement of pvT behaviour [50]

4.1 Specimens for wide angle X-ray scattering

Specimens for wide angle X-ray scattering (WAXS) were cut out from the central part of the prepared samples by using a rotary microtome Leica RM2255 supplied by Leica Microsystems (*Fig. 22*). The specimen dimension was 4 mm height and 7.5 mm width.

4.2 Specimens for Scanning Electron Microscopy

Specimens for scanning electron microscopy (SEM) were prepared from central part of the sawed off segments. Afterwards the specimens were etched by 1% solution of KMnO_4 in H_3PO_4 (85%) for 60 minutes.

4.3 Specimens for DSC analysis

The slices with thickness approx. 100 μm were cut out from central part of the sawed off segments using a rotary microtome Leica RM2255 supplied by Leica Microsystems (*Fig. 22*). The slices of weight of approx. 7 mg were put into the aluminous pan by tweezers and covered with the aluminous cover. The pan and the cover were crimped with a special tool supplied by Perkin-Elmer.

4.4 Specimens for determination of compressive properties

The prepared samples were grinded from both sides by using water cooled disk-type grinder with sand papers to straight cylinder shape. The specimen dimension was approx. 16 mm height and 7.5 mm width.



Fig. 22: Rotary microtome Leica 2255 [51]

5 ANALYZING METHODS AND DEVICES

5.1 Wide angle X-ray scattering

Wide angle X-ray scattering (WAXS) were performed with a X'PERT PRO MPD (Multi-Purposed Diffractometer) by PANanalytical company, this device is shown in *Fig. 23*. The diffractometer is equipped with CuK_α in reflection mode and nickel filter of thickness 0.2 mm. Radial scans of intensity vs. diffraction angle 2θ were recorded in the range of 7° to 30° by steps of 0.026° .



Fig. 23: Diffractometer X'PERT PRO MPD

5.2 Differential scanning calorimetry analysis

For the purpose of crystallization studies, a power-compensated differential scanning calorimeter Perkin-Elmer Pyris 1 was employed, it is shown in *Fig. 24*. The temperature calibration was performed using indium as a standard ($T_m = 156.6^\circ\text{C}$).

The prepared samples were heated from 50 up to 190°C with heating rate $10^\circ\text{C}/\text{min}$ to obtain melting temperature and enthalpy of heat fusion.



Fig. 24: Differential scanning calorimeter Perkin-Elmer Pyris 1

5.3 Scanning electron microscopy

In order to study morphology of the crystallized samples, a scanning electron microscope Vega-II LMU by Tescan Company USA, was employed, this device is shown in *Fig. 25*.



Fig. 25: Scanning electron microscope Vega-II LMU [52]

5.4 Compressive testing

Mechanical properties of crystallized samples were analyzed by compressive testing. The device INSTRON 8871 was employed, it is shown in *Fig. 26*. The compressive test was run at speed 1mm/min. This method was employed to determined values: modulus, compressive strain at tensile strength, and compressive stress at tensile strength.



Fig. 26: Compressive measurement INSTRON 8871

III. RESULTS AND DISCUSSION

6 HIGH PRESSURE CRYSTALLIZATION

Pressure-volume-temperature (pvT) technique was used to prepare the samples and at the same time to find out the crystallization behaviour, mainly crystallization temperatures (T_c) of each material. Five pressures were applied varying from 20 to 160 MPa. The typical sigmoidal crystallization curves of each material obtained by pvT100, i. e. dependence of specific volume on temperature, are shown in *Figs. 27-29*. It is well known that during crystallization the specific volume decreases as macromolecules integrate into crystallites. Crystallization temperatures were calculated from dilatometrics data, as a flex point and they are summarized in *Tab. 6* and graphically expressed in *Fig. 30*.

Tab. 6: Crystallization temperatures of PP, LCB-PP, and c-PP crystallized under different pressures

Pressure (MPa)	PP T_c (°C)	LCB-PP T_c (°C)	c-PP T_c (°C)
20	123	136	123
40	126	142	133
80	137	155	139
120	172	165	174
160	193	181	194

The results of high pressure crystallization exhibits that crystallization temperature raises with increasing pressure for all used materials (see *Fig. 30*). The crystallization curves of PP and c-PP possess an analogous form, thus the crystallization behaviour of such materials is more or less identical. However, in the case of LCB-PP the dependence of T_c on specific volume is significantly different. LCB-PP possesses higher T_c up to crystallization pressure 80 MPa as compared to other materials. Then, at pressure 120 and 160 MPa, the values of T_c of PP and c-PP exceed that of LCB-PP. Thus it can be said that under lower pressures LCB-PP crystallizes easily than PP (c-PP) while at higher pressures the situation is opposite, i.e. LCB-PP crystallizes hardly (slowly). The higher crystallization temperature of LCB-PP at common conditions (lower pressure) has been already published and has been assigned to long branches which can act as a nucleating agent and thus speed the crystallization [1]. On the other hand, under high pressures (120 MPa and above) the long chains can contrary slow the crystallization as there is no enough place to move and long chains represent a restrictions for implementing macromolecules into crystallites.

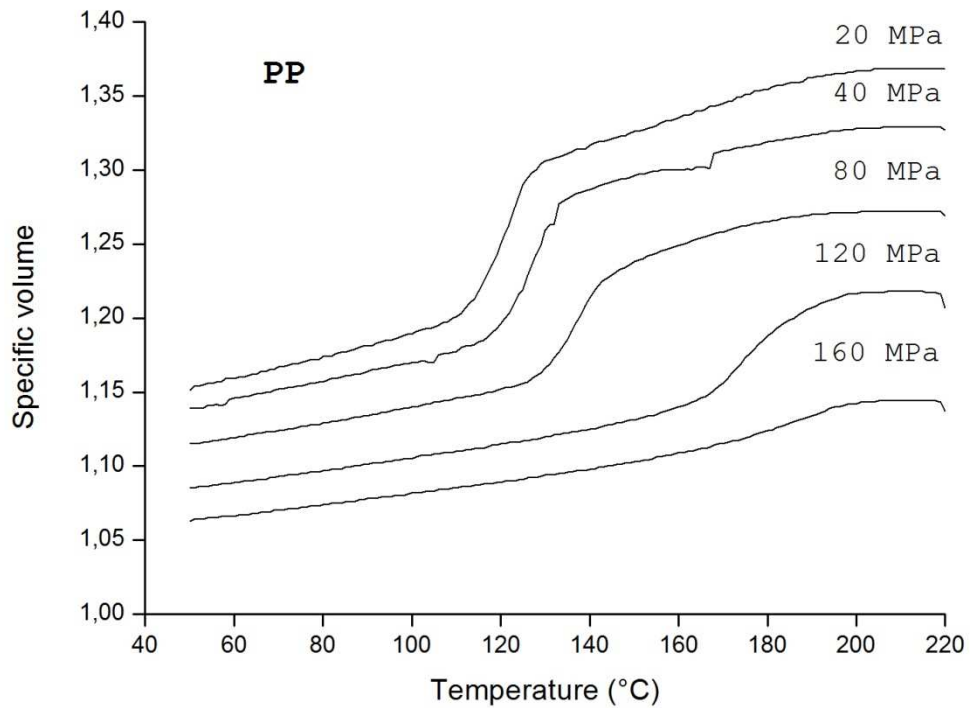


Fig. 27: The dependence of specific volume on temperature for PP crystallized under different pressures

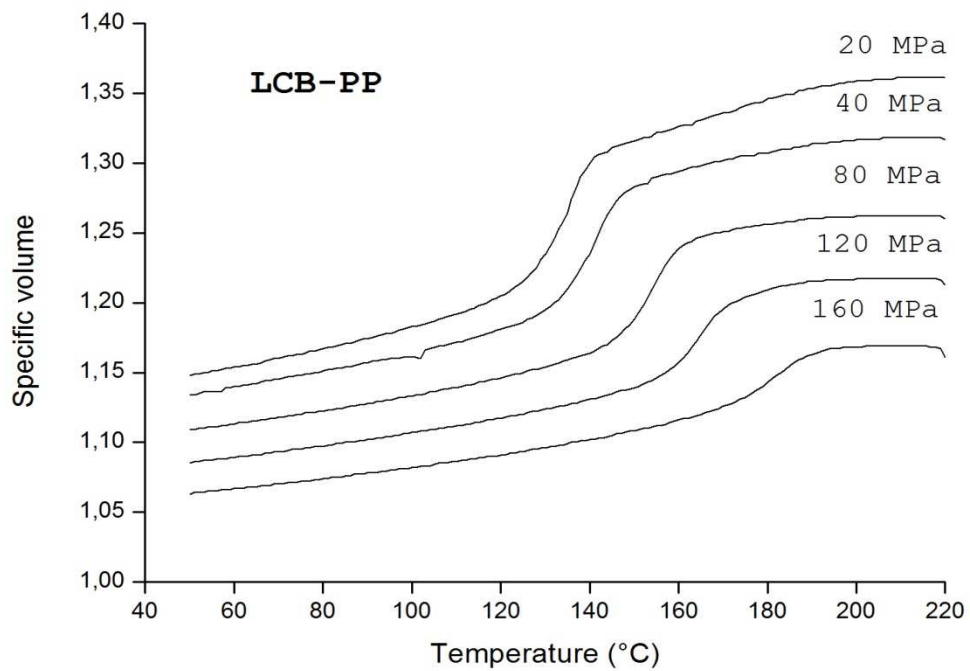


Fig. 28: The dependence of specific volume on temperature for LCB-PP crystallized under different pressures

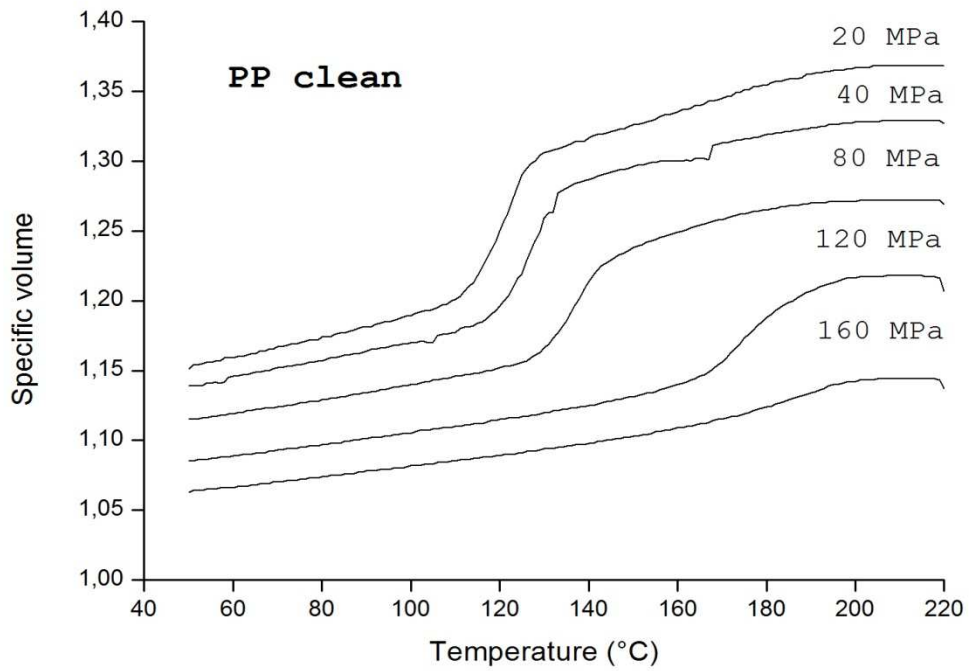


Fig. 29: The dependence of specific volume on temperature for *c*-PP crystallized under different pressures

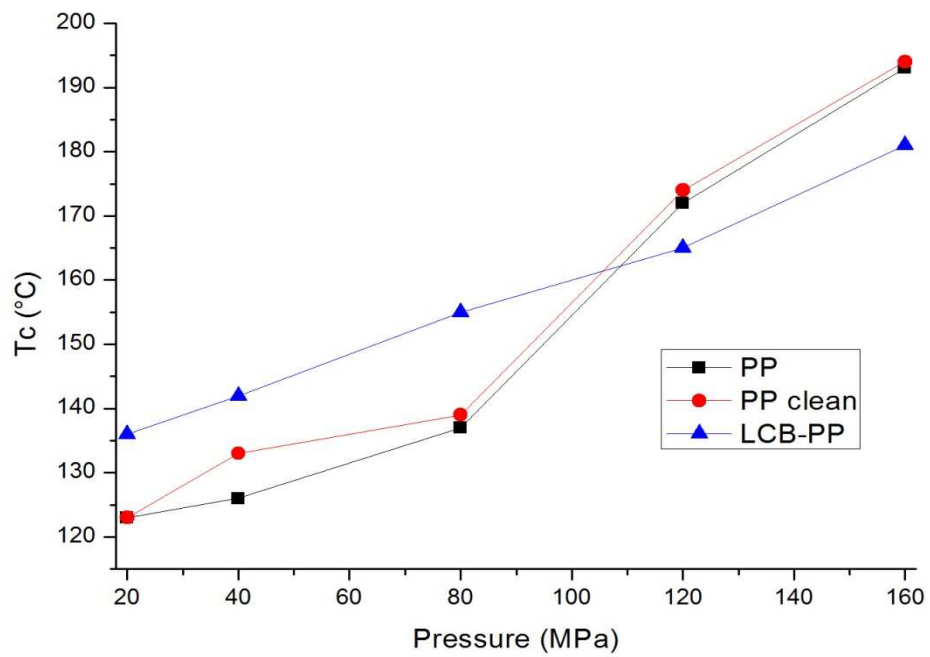


Fig. 30: Crystallization temperatures of PP, LCB-PP, and *c*-PP crystallized under different pressures

7 WIDE ANGLE X-RAY SCATTERING

Wide angle X-ray scattering was employed to observe a polymorphic composition of each material. The corresponding WAXS patterns are shown in *Figs. 31-33*. Here the typical reflections at around $2\theta = 14.2^\circ$, 17° and 18.8° corresponding to (110), (040) and (130) of α -form can be observed. With increasing pressure also reflection at $2\theta = 20.05^\circ$ corresponding to (117) of γ -form becomes distinct. From the diffraction patterns the values of crystallinity and γ -form content are calculated. The crystallinity is determined as the ratio of the integral intensities diffracted by a crystalline part (I_c) and total integral intensities (I) ($X_c=I_c/I$). The relative content of γ -form (G) in the γ/α crystalline system is calculated according to Pae as $G=H_\gamma/(H\alpha_3+H_\gamma).100\%$, where H_γ is the intensity of the (117) γ -reflection and $H\alpha_3$ is the intensity of the (130) α -reflection [53]. The values of relative content of γ -form and crystallinity are shown in *Tab. 7* and graphically expressed in *Figs. 34* and *35*.

Tab. 7: The relative content of γ -form and crystallinity of PP, LCB-PP, and c-PP crystallized under different pressures (%)

Pressure (MPa)	PP		LCB-PP		c-PP	
	X_c	γ -form	X_c	γ -form	X_c	γ -form
20	54	10	63	30	58	11
40	57	17	57	55	58	24
80	49	46	55	82	54	49
120	47	71	57	100	54	78
160	49	83	58	100	54	92

The prepared samples of each material consisted of only α - and γ -forms, β -form was not observed. The γ -form content increases with elevated pressure in all materials under study. Both PP and c-PP indicate very similar evolution of polymorphic composition with increasing crystallization pressure; the relative γ -form content is comparable. On the other hand, the LCB-PP has a higher tendency to crystallize into γ -form with elevated pressure than PP and c-PP; the relative γ -form content is significantly higher for all pressures. Moreover, at pressure 120 MPa the relative content of γ -form in such material reaches the maximum 100 %. The higher tendency to create γ -form under increased pressure has been already well described elsewhere [19] and is generally known. On the other hand, the crystallization of LCB-PP and its polymorphic composition is not fully understood yet. The data published so far [e.g. 54, 55, 56] indicated that when the fully isotactic sequences

(branches) are very short, iPP crystallizes into γ -form, whereas very long regular isotactic sequences (branches) generally crystallizes only into α -form. Weng analyzed the LCB structures in the LCB-PP in detail with ^{13}C NMR, and pointed out that the incorporation of LCB structures in the LCB-PP will bring stereo mistakes in isotactic backbone structures [30]. As a result, the LCB structure will influence the final phase structure of LCB-PP. In the work of Su et al. the higher tendency of LCB-PP to crystallize into γ -form has been proved [2]. However, in this work only the influence of T_c was studied, no pressure dependence is taken into account.

As can be seen in *Fig. 35* the crystallinity varies from sample to sample. In general, the crystallinity is higher in c-PP and LCB-PP, the common polypropylene possesses slightly lower values. According to results it can be also said that high pressure gently decreases the crystallinity in all samples. The higher crystallinity in c-PP in comparison with PP could be expected: the impurities in such material have been removed and thus there are fewer defects of crystallites.

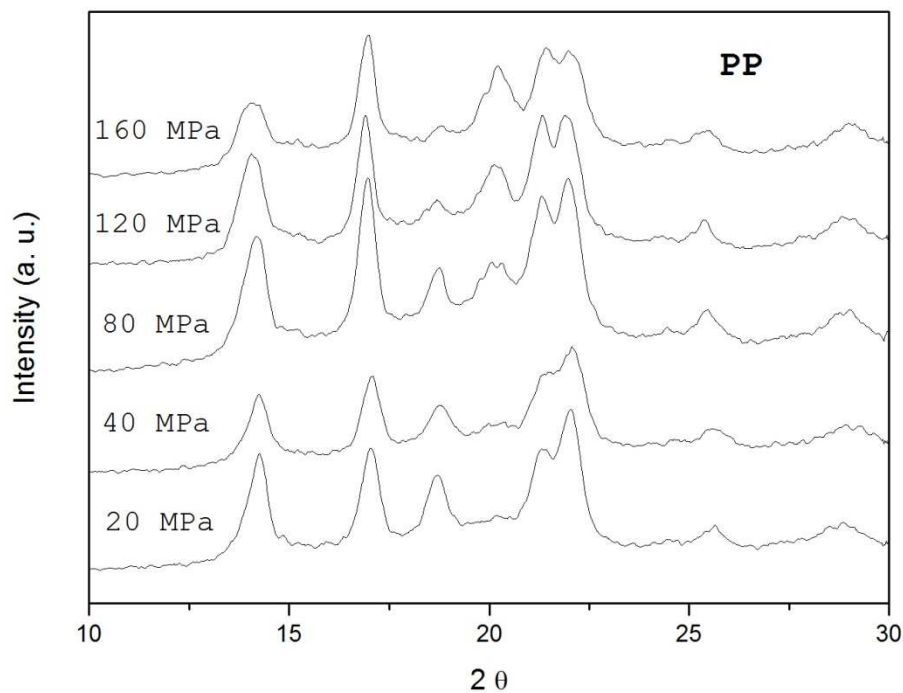


Fig. 31: Diffractograms of PP samples crystallized at elevated pressure

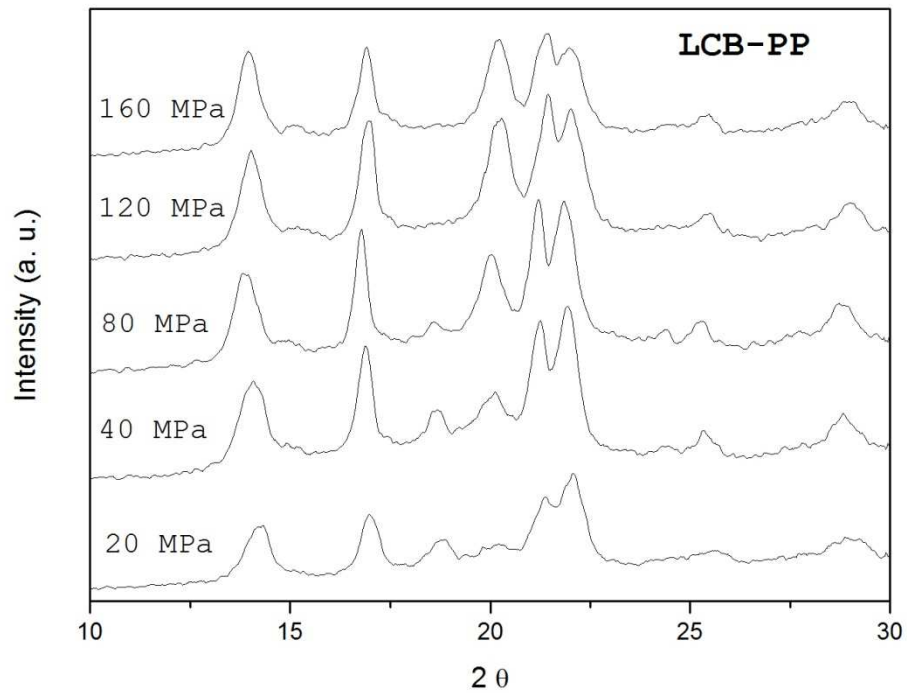


Fig. 32: Diffractograms of LCB-PP samples at elevated pressure

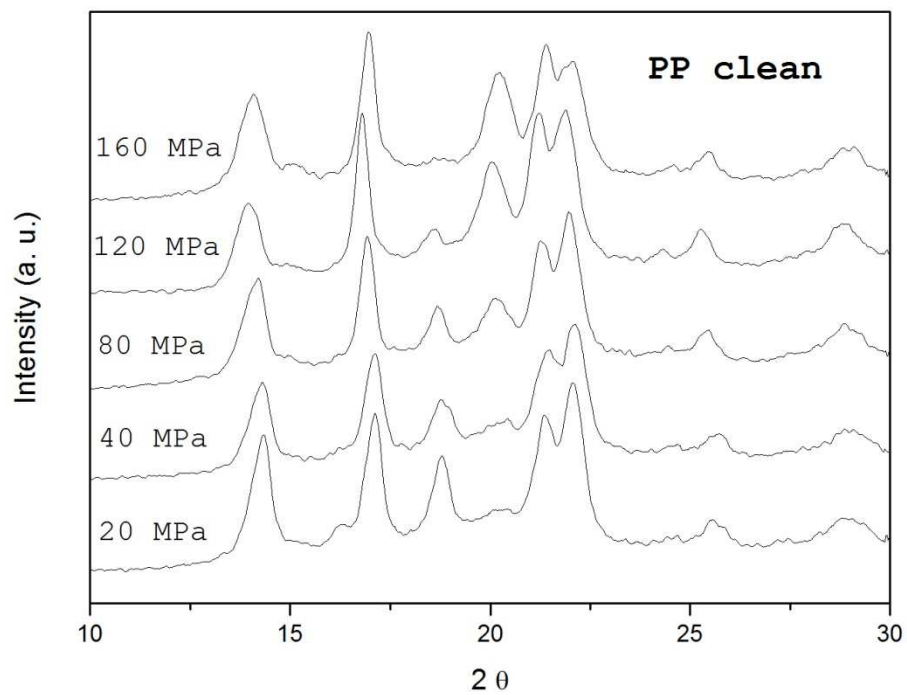


Fig. 33: Diffractograms of c-PP crystallized at elevated pressure

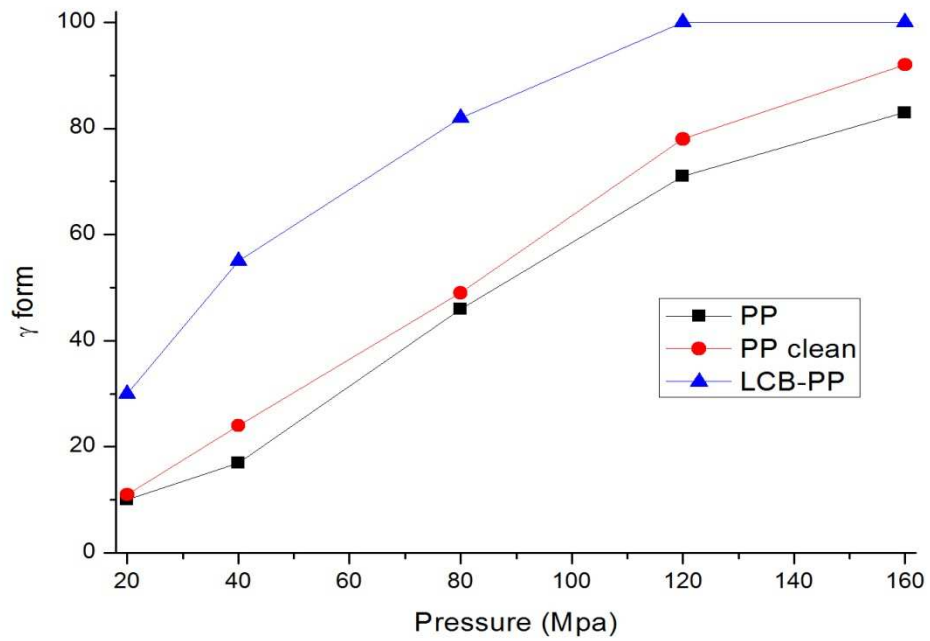


Fig. 34: The content of γ -form of PP, c-PP, and LCB-PP crystallized at elevated pressure

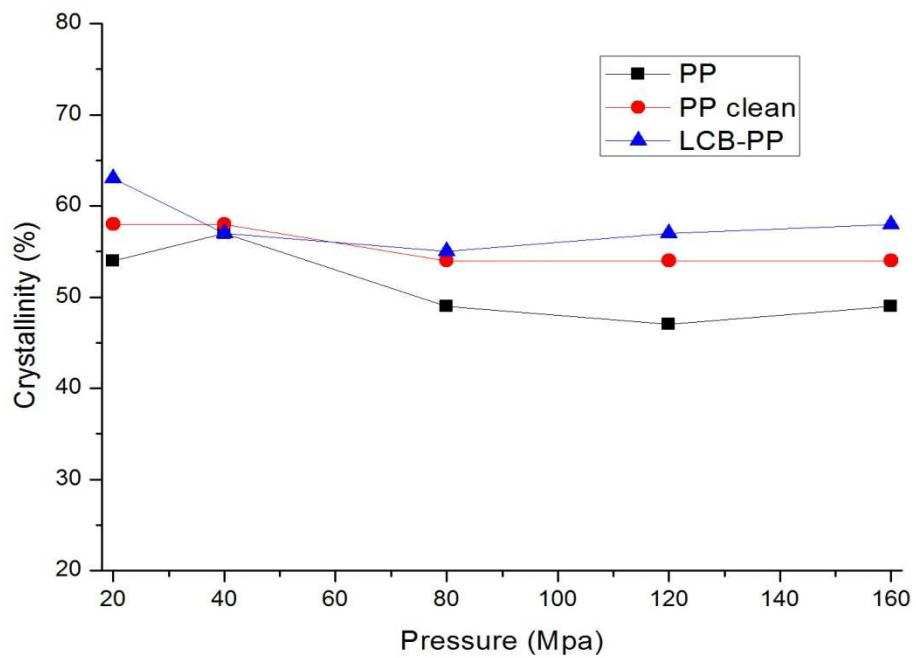


Fig. 35: The dependence of crystallinity of PP, c-PP, and LCB-PP crystallized at elevated pressure

8 DIFFERENTIAL SCANNING CALORIMETRY

Differential scanning calorimetry was used to observe the melting behaviour of high pressure crystallized samples.

Melting thermograms of all prepared samples are illustrated in *Figs. 36-38*. From the thermograms, melting temperature and melting enthalpy have been determined and the values are listed in *Tab. 8* and graphically expressed in *Figs. 39* and *40*. The melting temperature has been taken as a maximum of melting endotherm. In some cases the splitting of melting peak can be observed (e. g. LCB-PP, 120 MPa, see *Fig. 37*). In this case, two melting temperatures are indicated in the graph (*Fig. 39*).

It can be seen in *Figs. 36-38* that the melting peak becomes broader with increasing crystallization pressure applied. This is connected with the presence of γ -form in high pressure crystallized samples. This polymorph of iPP possesses lower melting temperature and thus in samples containing both α - and γ -forms the peak has onset at lower temperature and is significantly broader. In the case of LCB-PP, the broadening leads in splitting of the melting peak into two individual peaks corresponding to separate melting of both forms. Indeed, this material contains the highest portion of γ -form within the crystalline portion (see *Fig. 34*) as compared to other samples; even at pressures 120 and 160 MPa it is composed of only γ -form. Nevertheless, the doubling of the peak is observed also in these cases. It can be connected with the recrystallization of γ -form into α -form. The γ -form is metastable and can melt and recrystallize into α -phase under heating. Very small additional peak at low temperature (approx. 150 °C) in c-PP thermogram is most probably connected with melting of trigonal β -form which has identical melting point. However, WAXS analysis did not revealed the presence of such polymorph in the material. Thus, it might be caused by $\alpha\alpha$ -recrystallization which can also occur during melting of iPP. The less perfect α_1 -form can recrystallize into better ordered α_2 -form [17]. At higher pressures this very small peak disappears as the main melting peak is broader and broader and can overlap it.

Fig. 39 shows the evolution of melting temperature with increasing crystallization pressure. The highest values are observed in c-PP while the lowest in LCB-PP. The melting temperature is connected with the lamellae thickness [57]. Thus it can be predicted that c-PP contains the thick lamellae and perfect crystallites while LCB-PP consists of thin lamellae and crystallites with number of defects. Moreover, it has been already published that the crystallites of γ -form in LCB-PP include a large amount of defects [58].

Fig. 40 shows the evolution of melting enthalpy with increasing crystallization pressure. Total enthalpy of melting is the relative area of the melting peaks. As can be seen, generally the melting enthalpy decreases with increasing pressure. This is in good agreement with data from WAXS (Fig. 35): the value of melting enthalpy reflects the value of crystallinity which decreases with raising pressure. Among the three samples the highest values of melting enthalpy is observed in c-PP which indicate its highest crystallinity. This is proved also by WAXS, however, similar values of crystallinity are observed for both c-PP and LCB-PP which is not indicated in DSC data. The problem could be found in the evaluation method of melting enthalpy, which is affected by human factor. Moreover, the value of melting enthalpy of c-PP crystallized at the lowest pressure 20 MPa seems to be yawing and thus cannot be taken into account. In general, WAXS data are considered as more predicative.

Tab. 8: Melting temperature ($^{\circ}\text{C}$) and total enthalpy of melting (J/g) of PP, LCB-PP, and c-PP crystallized at elevated pressure

Pressure (MPa)	PP		LCB-PP		c-PP	
	T_m	ΔH_m	T_m	ΔH_m	T_m	ΔH_m
20	161,1	106,7	159,4	109,9	162,1	98,6
40	160,4	102,6	159,2	107,2	162,6	112,5
80	160,6	102	159,4	103,5	162,3	111,4
120	160,2	99,4	158,8	97,3	161,7	108,5
160	159,7	97,9	158,8	97,8	161	101,4

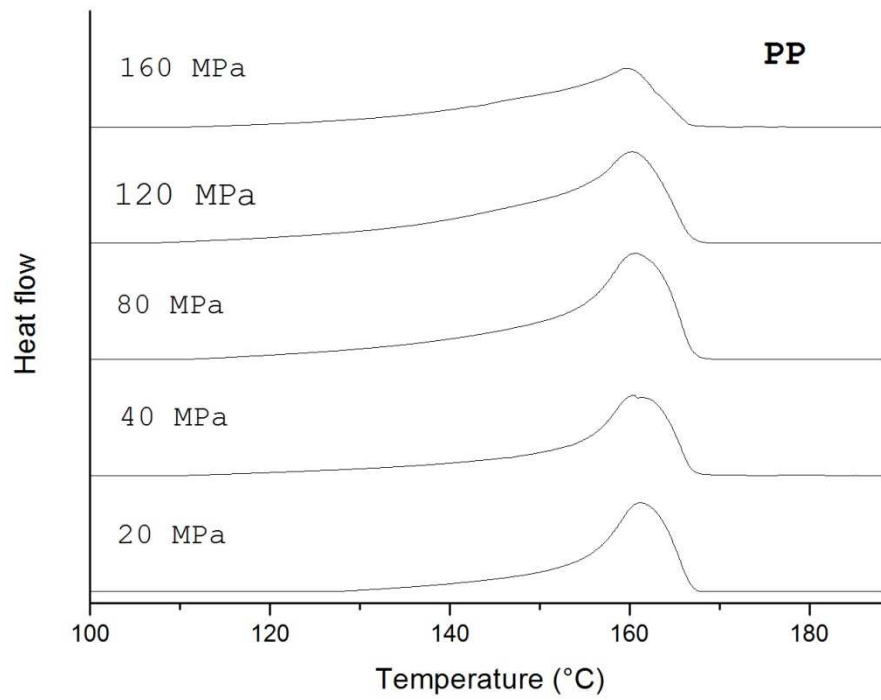


Fig. 36: Melting thermograms of PP crystallized at elevated pressure

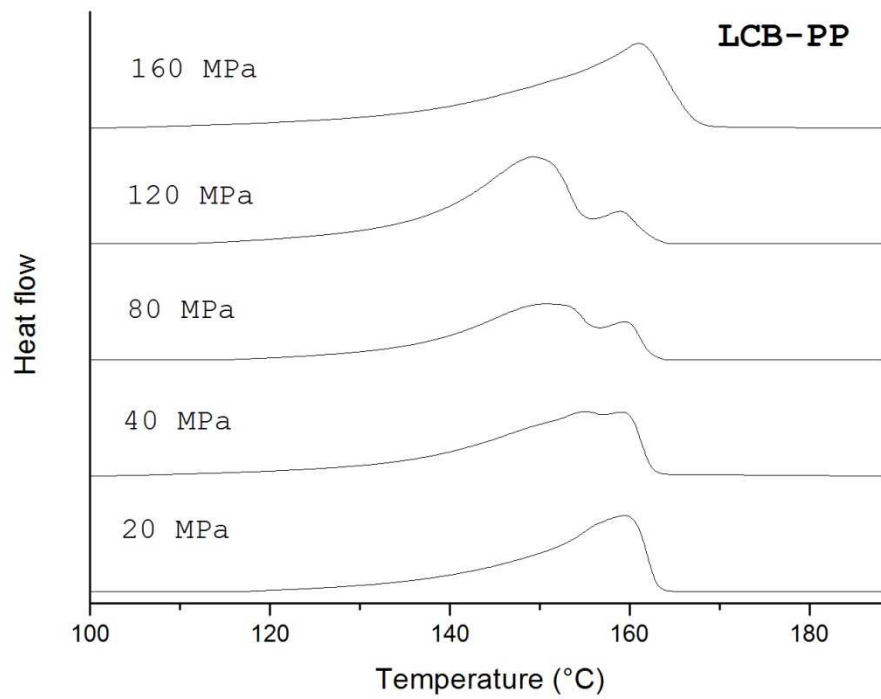


Fig. 37: Melting thermograms of LCB-PP crystallized at elevated pressure

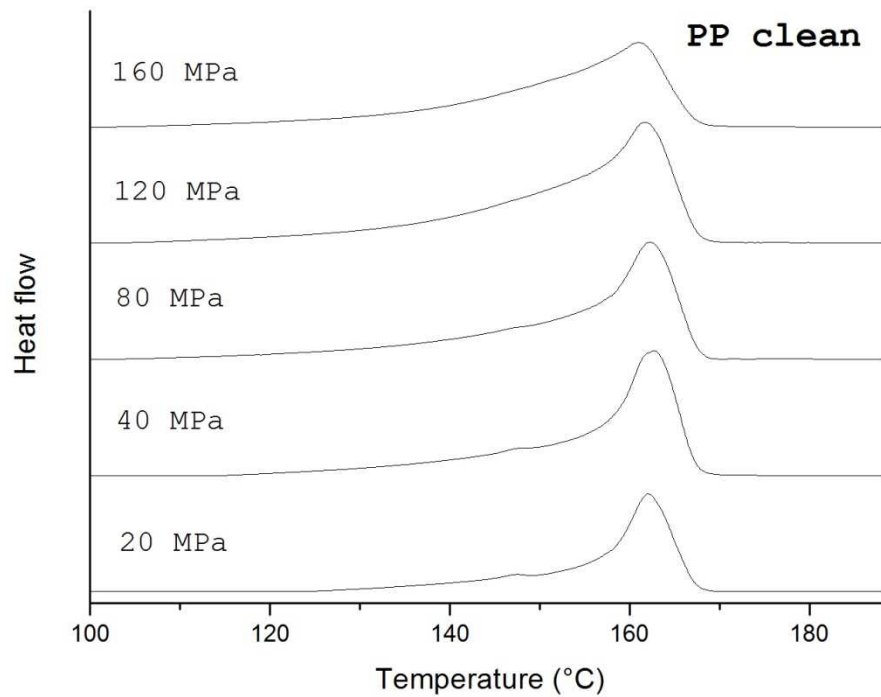


Fig. 38: Melting thermograms of *c*-PP crystallized at elevated pressure

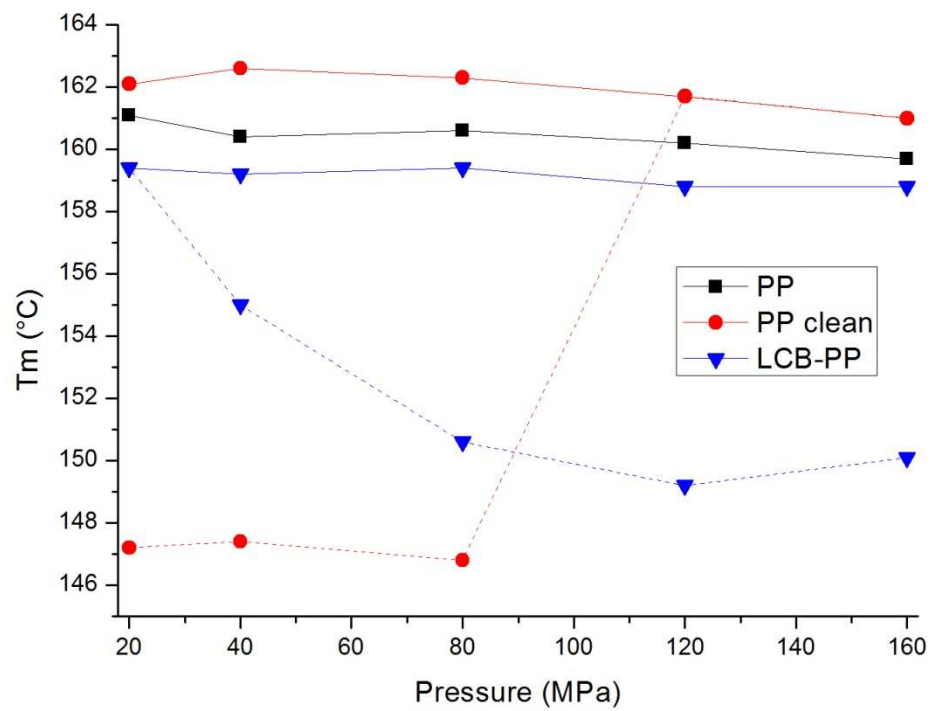


Fig. 39: The evolution of melting temperature at elevated pressure

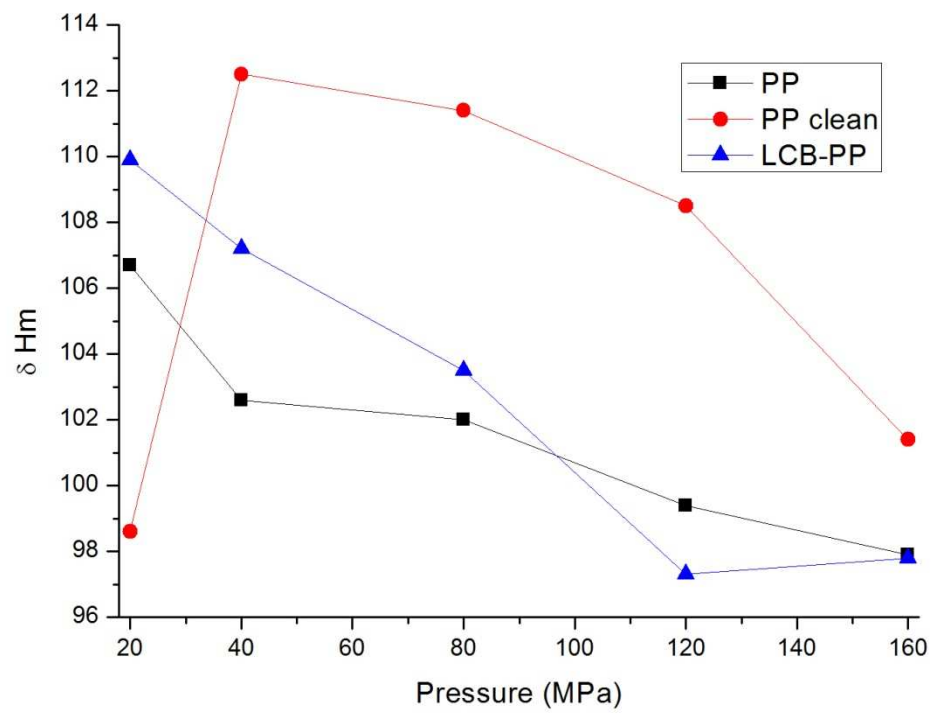


Fig. 40: The evolution of total enthalpy of melting at elevated pressure

9 SCANNING ELECTRON MICROSCOPY

The morphology of the prepared samples crystallized at elevated pressure is illustrated in micrographs taken by scanning electron microscope at different magnitudes (*Figs. 41-43*).

Fig. 41 shows the structure of the materials crystallized under 20, 80 and 160 MPa at the lowest magnitude. As can be seen, the typical spherulitic structure formed in PP and c-PP. Spherulites are large and clearly visible with distinct boundaries (mainly at low pressure). The boundaries of the spherulites are better seen in *Fig. 42* where greater magnitude has been used. According to WAXS analysis (see *Fig. 34*) the materials consists predominantly of γ -phase at high pressure (160 MPa). Indeed, the spherulites seem to be quite different. On the other hand, the morphology of LCB-PP does not show typical spherulites, the crystalline objects are very small and each crystallite cannot be defined (*Fig. 43*). The LCB-PP forms some type of aggregates which have corporate nuclei from which the arrays grow up. The arrays are probably composed of radial (mother) lamellae which seem to be overgrown epitaxially [4]. These details are nevertheless not evident from the scans most probably due to insufficient etching. *Fig. 43* shows the structure of LCB-PP in detail.

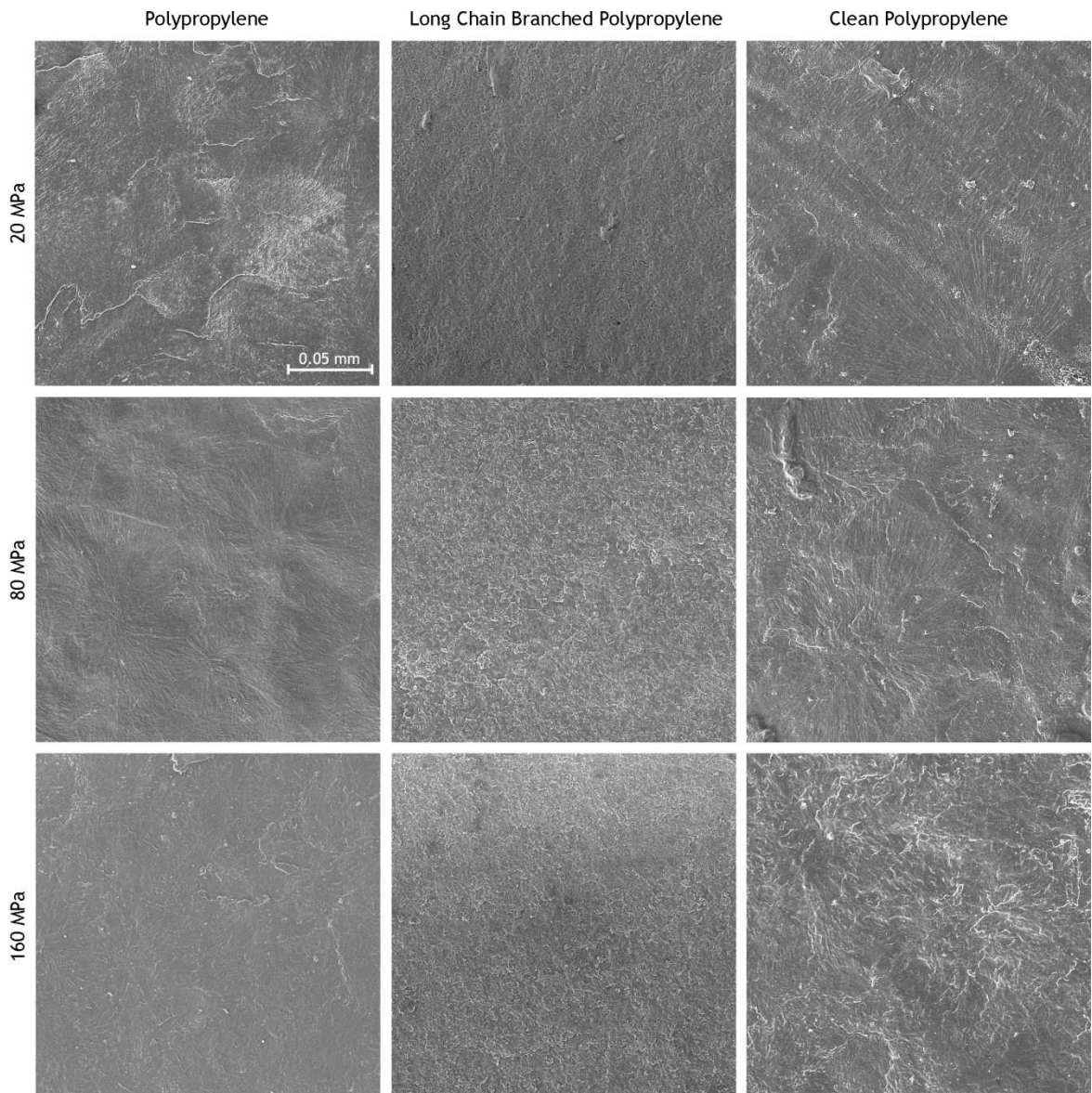


Fig. 41: Morphology of PP, LCB-PP, and c-PP samples crystallized under different pressures by SEM (magnification 1 000x)

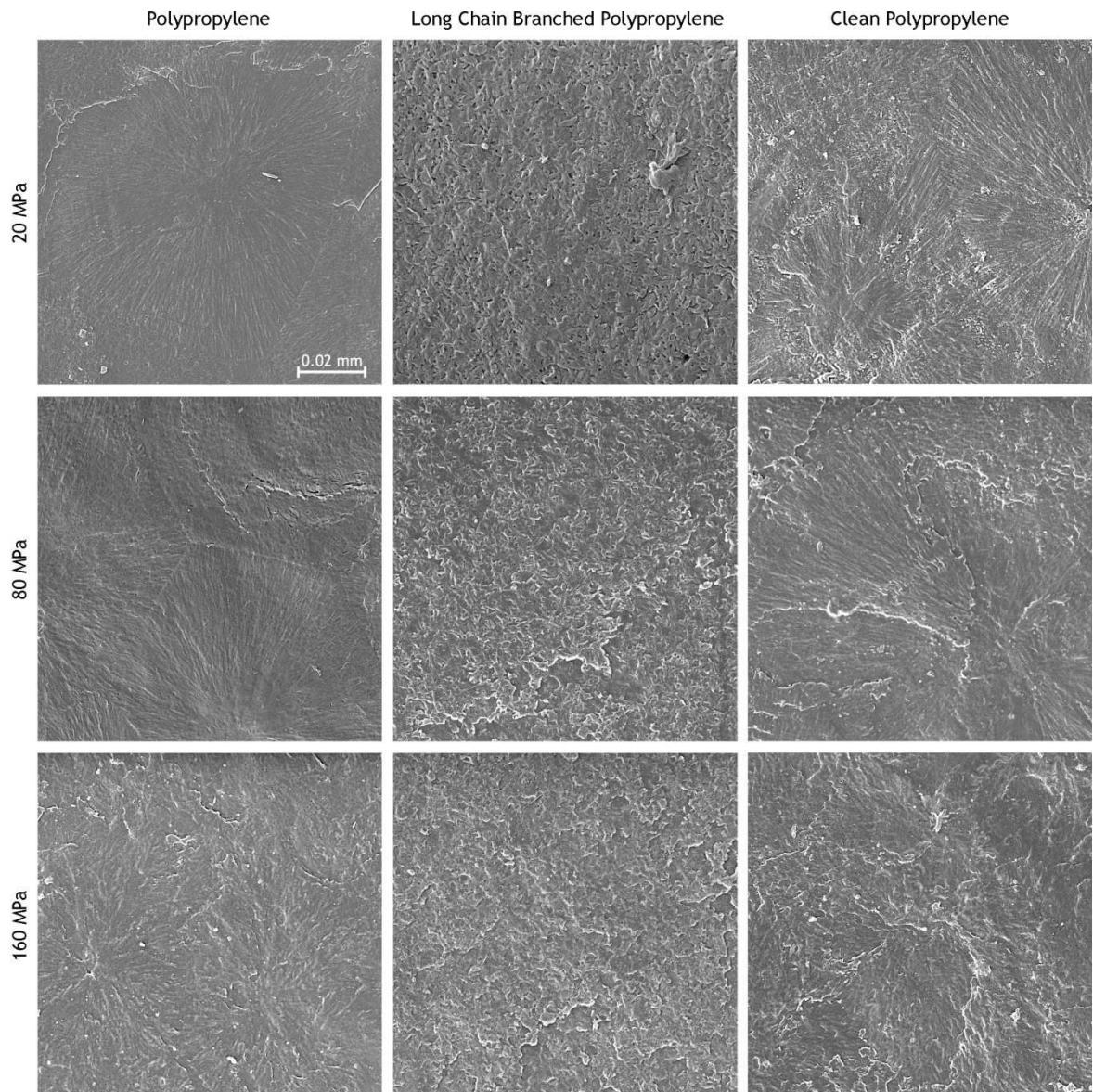


Fig. 42: Morphology of PP, LCB-PP, and c-PP samples crystallized under different pressures by SEM (magnification 2 000x)

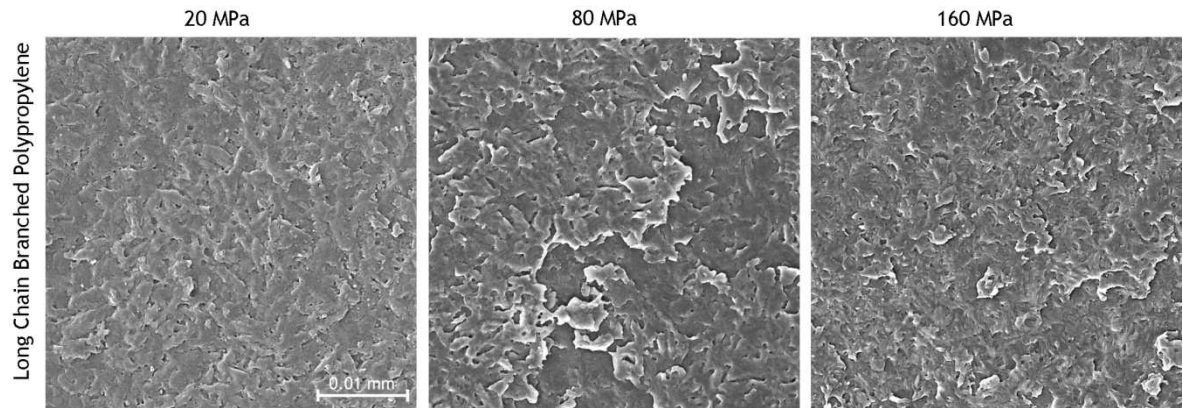


Fig. 43: Morphology of LCB-PP crystallized at elevated pressure.

10 COMPRESSIVE TESTING

The mechanical properties of samples crystallized at elevated pressure were determined via compressive testing. The results of compressive testing (tensile stress, tensile strain and E-modulus) are shown in *Tabs. 9-11* and graphically expressed in *Figs. 44-46*.

Tab. 9 and *Fig. 44* show values of compressive stress at tensile strength for samples crystallized under different pressures. Generally, there is not a significant dependence, only an increasing trend of compressive stress with elevating pressure can be observed in case of LCB-PP. On the contrary PP and c-PP possess decreasing trend of compressive stress with elevating pressure. However, the values are very similar and to speak about trend is quite courageous. What can be also seen from the graph is that PP possesses slightly lower values as compared to c-PP and LCB-PP.

The values of compressive strain at tensile strength for samples crystallized under different pressures are shown in *Tab. 10* and *Fig. 45*. Generally the highest values are observed for PP and the lowest for c-PP. There is a very slightly increasing trend of compressive strain with elevating pressure for all materials. The most increasing trend is most pronounced for LCB-PP, which might be associated with the highest increase of γ -form portion with increasing crystallization pressure in such material. However, the standard deviations are too high and thus the data are misrepresented.

The values of modulus (automatic) for samples crystallized under different pressures are shown in *Tab. 11* and *Fig. 46*. The lowest values of modulus possess PP and the highest were found out for c-PP. However, again no significant trend could be derived from the results; the values change with the pressure without clear tendency.

The lack of statistical significance is probably a consequence of the shapes and dimensions of prepared samples. Thus the results from compressive testing have not been accepted as a relevant in this study.

Tab. 9: Compressive stress at tensile strength for PP, LCB-PP, and c-PP crystallized at elevated pressure

Pressure (MPa)	Compressive stress at tensile strength (MPa)					
	PP		LCB-PP		c-PP	
	Mean	Standard deviation	Mean	Standard deviation	Mean	Standard deviation
20	52,89	1,45	55,05	1,32	57,17	1,10
40	50,78	1,42	53,75	1,53	59,06	0,91
80	48,63	0,71	56,74	2,67	54,07	2,54
120	56,59	6,11	55,76	1,42	52,94	0,85
160	48,45	6,94	57,92	4,01	53,25	3,27

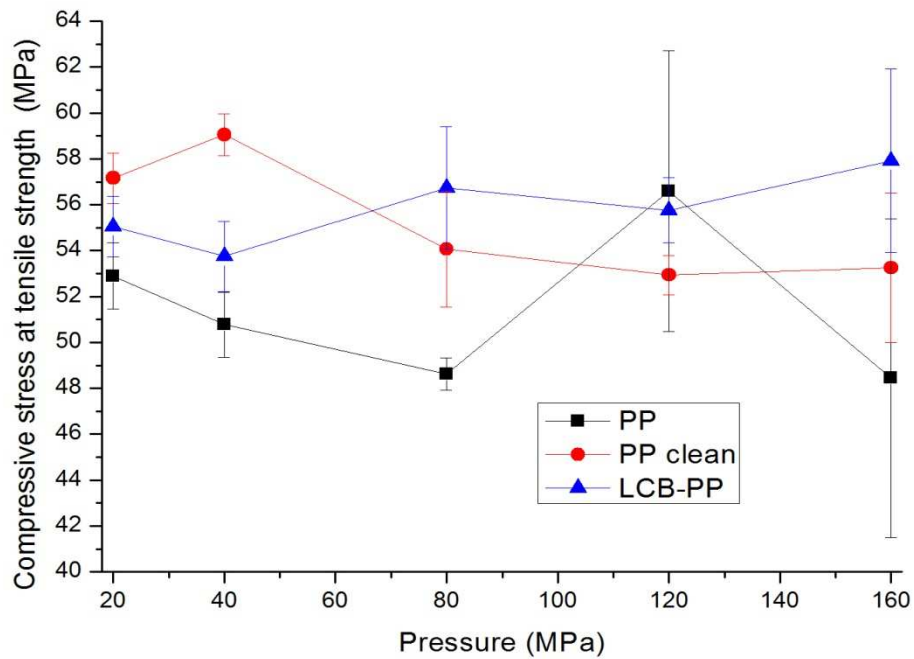


Fig. 44: The dependence of compressive stress at tensile strength on elevating pressure

Tab. 10: Compressive strain at tensile strength for PP, LCB-PP, and c-PP crystallized at elevated pressure

Pressure (MPa)	Compressive strain at tensile strength (mm/mm)					
	PP		LCB-PP		c-PP	
	Mean	Standard deviation	Mean	Standard deviation	Mean	Standard deviation
20	0,29	0,07	0,13	0,10	0,18	0,05
40	0,26	0,10	0,13	0,08	0,22	0,02
80	0,25	0,11	0,31	0,11	0,19	0,02
120	0,36	0,15	0,28	0,09	0,19	0,02
160	0,29	0,16	0,30	0,18	0,28	0,16

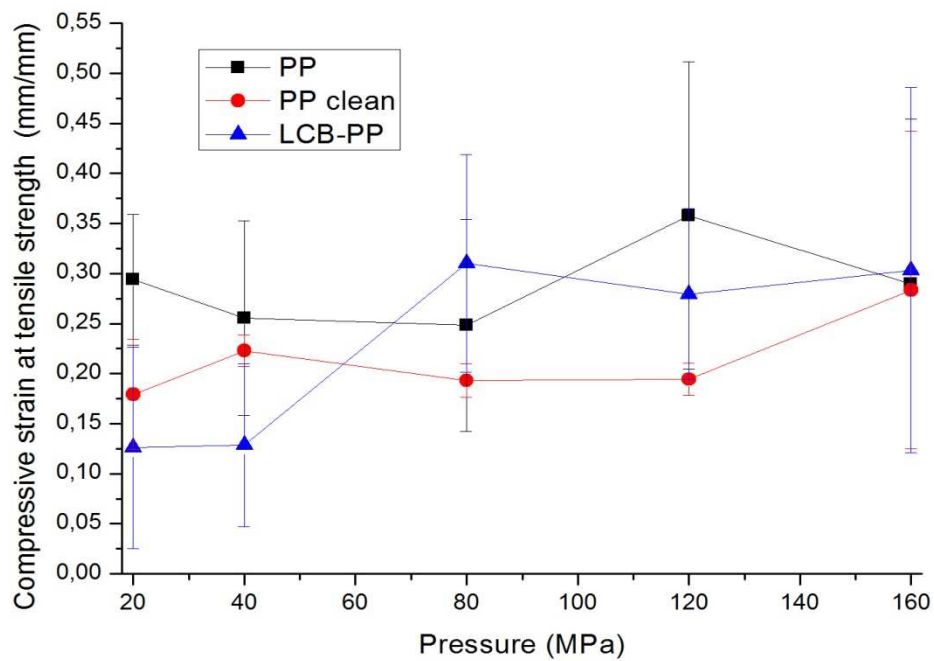


Fig. 45: The dependence of compressive strain at tensile strength on elevating pressure

Tab. 11: Modulus (automatic) for PP, LCB-PP, and c-PP crystallized at elevated pressure

Pressure (MPa)	Modulus (automatic) (MPa)					
	PP		LCB-PP		c-PP	
	Mean	Standard deviation	Mean	Standard deviation	Mean	Standard deviation
20	814,12	87,11	1265,28	217,32	1225,87	157,09
40	958,08	97,35	1264,67	124,74	1417,05	59,04
80	891,69	164,43	972,84	214,54	1158,83	98,40
120	700,57	235,54	1038,12	195,83	1299,59	238,88
160	720,14	138,51	1398,98	118,90	1268,02	227,84

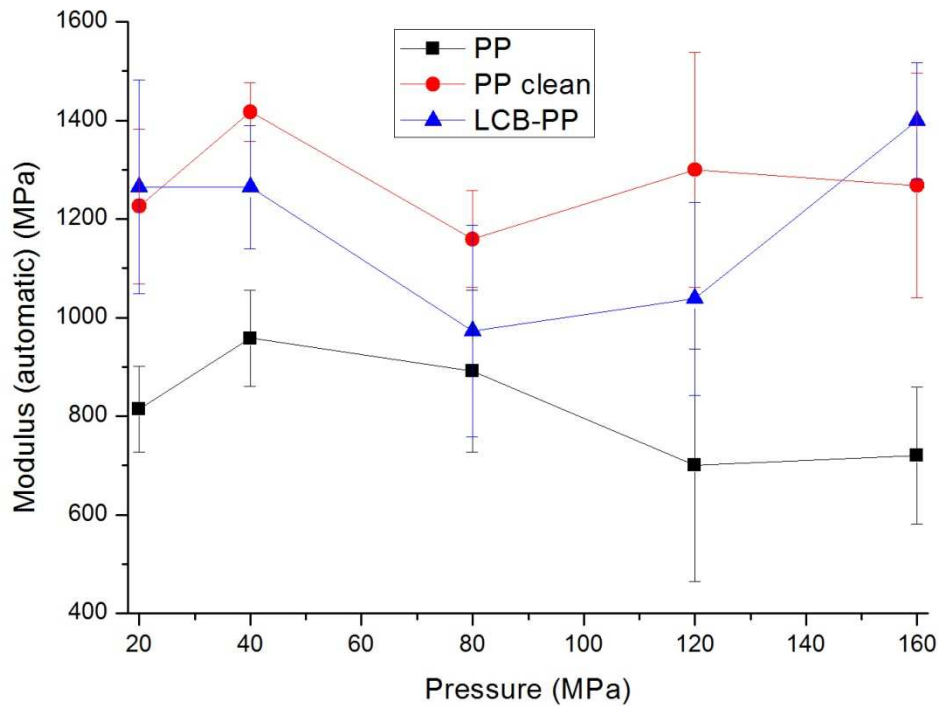


Fig. 46: The dependence of Modulus (automatic) on elevating pressure

CONCLUSION

This Master thesis deals with a study of crystallization of long chain branched polypropylene under increased pressure. Three different polypropylenes (PP homopolymer, LCB-PP and clean PP) were crystallized under increased pressure and then the structure and mechanical properties were investigated. The structure was evaluated via several methods, namely wide angle X-ray scattering, differential scanning calorimetry, scanning electron microscopy. Mechanical properties were determined via compressive testing.

Pressure-volume-temperature (pvT) technique was used to prepare the samples of each material and find out the crystallization temperatures. The results of high pressure crystallization exhibits that crystallization temperature raises with increasing pressure for all used materials. Under lower pressures LCB-PP crystallizes easily than PP and c-PP, it is caused by long branches which act as a nucleating agent. The opposite situation is at higher pressures (120 MPa and above), the long branches slow the crystallization, because there is no enough place to move and macromolecules cannot implement into crystallites easily.

The polymorphic composition of each material was observed by wide angle X-ray scattering. The results indicate that the prepared samples consisted of only α - and γ -forms, β -form was not observed. γ -form content increases with elevated pressure in all materials under study. The most significant it is in case of LCB-PP, which reaches the maximum 100% at pressure 120 MPa. The crystallinity is higher in LCB-PP and c-PP than in common PP.

The melting thermograms of differential scanning calorimetry showed that the melting peak becomes broader with increasing crystallization pressure, which is connected with the presence of γ -form. The highest values of melting temperature were observed for c-PP while the lowest for LCB-PP, which is caused by consistence of thin lamellae and crystallites with number of defects. The melting enthalpy decreases with increasing pressure.

Scanning electron microscopy provided interesting insight into the morphology of all materials. Spherulites are large and clearly visible with distinct boundaries in PP and c-PP. The morphology of LCB-PP does not show typical spherulites, the crystalline objects are significantly smaller and not distinctly separated each other.

The results from compressive testing have not been accepted as a relevant in this study, because of the lack of statistical significance.

To conclude, the high pressure crystallization does significantly influence the morphology of all materials under study. The results in this work could be a way for further investigation of LCB-PP.

REFERENCES

- [1] TIAN, J., YU, W., ZHOU, CH.: J. Appl. Polym. Sci., vol. 104, 2007, pp. 3592-3600
- [2] SU, Z., et al.: Polymer, vol. 48, 2007, pp. 870-876
- [3] TIAN, J., YU, W., ZHOU, CH.: Polymer, vol. 47, 2006, pp. 7962-7969
- [4] ZENG, W., WANG, J., FENG, Z., DONG, J. Y., YAN, S.: Colloid Polym. Sci., vol. 284, 2005, pp. 322-326
- [5] REITER, G., STROBL, G. R.: Progress in understanding of polymer crystallization, Springer, 2007, ISBN 978-3540473053
- [6] BASSETT, D. C.: Principles of polymer morphology, Cambridge University Press, 1st edition, 1981, ISBN 978-0521232708
- [7] MERSMANN, A.: Crystallization technology handbook, CRC Press, 2nd revised edition, 2001, ISBN 978-0824705282
- [8] JONES, A. G.: Crystallization process systems, A Butterworth-Heinemann Title, 2002, ISBN 978-0750655200
- [9] EBEWELE, R. O.: Polymer science and technology, CRC Press, 1st edition, 2000, ISBN 978-0849389399
- [10] MAIER, C., CALAFUT, T.: Polypropylene: The definitive user's guide and databook, Plastic Design Library, 1998, ISBN 1-884207-58-8
- [11] RYBNIKÁŘ, F.: Makromolekulární chemie I, VUT Brno, 1987, 91 p.
- [12] KARGER-KOCSIS, J.: An A-Z reference, Dordrecht, Kluwer Academic Publishers, 1999, 0-412-80200-7
- [13] Maltese cross patterns [online], [cited: 10. 4. 2010], <http://gertrude-old.case.edu/276/materials/145/14.htm>
- [14] SEYMOUR, R. B., CARRAHER, CH. E.: Polymer chemistry: an introduction, M. Dekker, 2nd edition, 1988, ISBN 9780824777814
- [15] WATANABE, K., et al.: Polymer, vol. 44, 2003, pp. 5843-5849
- [16] SPERLING, L. H.: Introduction to physical polymer science, Wiley-Interscience, 3rd edition, 2001, ISBN 0-471-329221-5

- [17] KARGER-KOCSIS, J.: Polypropylene: Structure, blends and composites, London: Chapman & Hall, 1995, ISBN 0-412-58430-1
- [18] RAAB, M., KOTEK, J., BALDRIAN, J., GRELLMANN, W.: J Appl. Polym. Sci., vol. 69, 1998, pp. 2255-2259
- [19] MEZGHANI, K., PHILLIPS, P. J.: Polymer, vol. 38, no. 23, 1997, pp. 5725-5733
- [20] DIMESKA, A., PHILLIPS, P. J.: Polymer, vol. 47, 2006, pp. 5445-5456
- [21] AIZENSHTEIN, E. M.: Fibre Chemistry, vol. 40, no. 5, 2008, pp. 399-405
- [22] ALGER, S. M.: Polymer science dictionary, Chapman & Hall, 1989, ISBN 0-412-60870-7
- [23] BRYDSON, J.: Plastics materials (7th edition), Butterworth-Heinemann, 1999, ISBN 078-0750641326
- [24] PAUKSZTA, D., GARBARZCYK, J.: Crystallization of isotactic polypropylene with β -nucleating agents under elevated pressure, Poznan, University of Technology, 2007
- [25] LEZAK, E., BARTZAK, Z.: Fibres and Textiles in Europe, vol. 13, no. 5 (53), 2005, pp. 51-56
- [26] KOTEK, J., RAAB, M., BALDRIAN, J., GRELLMANN, W.: J. Appl. Polym. Sci., vol. 85, 2002, pp. 1174-1184
- [27] PHILLIPS, P. J., MEZGHANI, K.: Polypropylene, isotactic (polymorphism), CRC Press, 1996
- [28] MEILLE, S. V., BRUCKNER, S., PORZIO, W.: Macromolecules, vol. 23, 1990, pp. 4114-4121
- [29] MLEZIVA, J., ŠŇUPÁREK, J.: Polymery – výroba, struktura, vlastnosti a použití, 2. Vydání, Sobotáles, 2000, 544 p., ISBN 80-85920-72-7
- [30] WENG, W., HU, W., DEKMEZIAN, A. H., RUFF, CH. J.: Macromolecules, vol. 35, 2002, pp. 3838-3843
- [31] LANGSTON, J. A., et al.: Macromol. Symp., vol. 260, 2007, pp. 34-41
- [32] RATZSCH, M. et al.: Prog. Polym. Sci., vol. 27, 2002, pp. 1195-1282
- [33] LUGAO, A. B., et al.: Radiat. Phys. Chem., vol. 76, 2007, pp. 1691-1695

- [34] KRAUSE, B. STEPHAN, S., VOLKLAND, D., VOIGT, L., HAUSSLER, L., DORSCHNER, H.: J. Appl. Polym. Sci., vol. 99, 2006, pp. 260-265
- [35] LAGENDIJK, R. P., HOGT, A. H., BUIJTENHUIJS, A., GOTSIS, A. D.: Polymer, vol. 42, 2001, pp. 10035-10043
- [36] YU, F., et al.: Eur. Polym. J., vol. 45, 2009, pp. 2110-2118
- [37] GOTSIS, A. D., ZEEVENHOVEN, B. L. F., HOGT, A. H.: Polym. Eng. Sci., vol. 44, no. 5, 2004, pp. 973-982
- [38] [online], [cited: 20. 4. 2010], <http://www.borealisgroup.com>
- [39] FANG, Y., SADEGHI, F., FLEURET, G., CARREAU, P. J.: Can. J. Chem. Eng., vol. 86, 2008, pp. 6-14
- [40] TISSUE, B. M.: X-ray Diffraction, 2000, [online], [cited: 24. 4. 2010], <http://elchem.kaist.ac.kr/vt/chem-ed/diffract/xray.htm>
- [41] KOO, J. H.: Polymer nanocomposites; processing, characterization, and applications, McGraw-Hill, New York, 2006, ISBN 0-07-145821-2
- [42] MARTON, L.: Polymers, vol. 16, Academic Press Inc, 1980
- [43] MULDER, M.: Basic principles of membrane technology, 2nd edition, Kluwer Academic Publishers, 1997, ISBN 0-7923-4248-8
- [44] LYMAN, CH. E., et al.: Scanning electron microscopy, X-ray microanalysis, and analytical electron microscopy, Plenum Press, New York, 1990, ISBN 0-306-43591-8
- [45] SCHEIRS, J.: Compositional and failure analysis of polymers – A practical approach, John Wiley and Sons, 2000, ISBN 0-471-62572-8
- [46] CHEREMISINOFF, N. P.: Polymer characterization – laboratory techniques and analysis, Notes Publications, 1996, ISBN 0-8155-1403-4
- [47] DEAN, J. A.: The analytical chemistry handbook, McGraw Hill, New York, 1995, pp. 15.1-15.5
- [48] Schematic diagram of differential scanning calorimetry [online], [cited: 22. 4. 2010], <http://evitherm.athena.as/>

- [49] MALKIN, A. Y.: Experimental methods of polymer, English translation, Mir Publishers, 1983
- [50] POTSCH, G., MICHAELI, W.: Injection molding – An introduction, 2nd edition, Carl Hanser Verlag, 2008, ISBN 978-446-40635-3
- [51] Rotary Microtome Leica 2255 [online], [cited: 22. 4. 2010], <http://www.leica-microsystems.com/products/by-application/materials-testing/sectioning/rotary-microtomes/details/product/leica-rm2255/>
- [52] Scanning Electron Microscope Vega-II LMU (Tescan USA), Laborator de Analize Morfologice La Scara Nanometrica [online], [cited: 27. 4. 2010], <http://www.imt.ro/nanomorph/resurse.php>.
- [53] PAE, K. D.: J. Appl. Phys., vol. 39, 1968, pp. 4959-4968
- [54] ALAMO, R. G., KIM, M. H., GALANTE, M. J., ISASI, J. R., MANDELKERN, L.: Macromolecules, vol. 32, 1999, pp. 4050-4064
- [55] VANDERHART, D. L., ALAMO, R. G., NYDEN, M. R., KIM, M. H., MANDELKERN, L.: Macromolecules, vol. 33, 2000, pp. 6078-6093
- [56] THOMANN, R., SEMKE, H., MAIER, R. D., THOMANN, Y., SCHERBLE, J., MULHAUPT, R., et al.: Polymer, vol. 42, 2001, pp. 4597-4603
- [57] HOFFMAN, J.D., WEEKS, J. J.: J. Chem. Phys., vol. 37, 1962, pp.1723-1742
- [58] AURIEMMA, F., DE ROSA, C., BOSCATO, T., CORRADINI P.: Macromolecules, vol. 34, 2001, pp. 4815-4826

LIST OF SYMBOLS

PP	Polypropylene
iPP	Isotactic polypropylene
LCB-PP	Long chain branched polypropylene
HMS-PP	High melt strength polypropylene
α	Monoclinic crystalline form
β	Trigonal crystalline form
γ	Orthorombic crystalline form
pvT	Pressure-volume-temperature
T_c	Crystallization temperature ($^{\circ}\text{C}$)
T_m	Melting temperature ($^{\circ}\text{C}$)
T_g	Glass transition temperature ($^{\circ}\text{C}$)
X_t	Volume fraction of crystalline material
K	Constant of nucleation from Avrami equation (s^{-n})
n	Constant of growth from Avrami equation
WAXD	Wide angle X-ray diffracting
DSC	Differential scanning calorimetry
SEM	Scanning electron microscopy
TEM	Transmission electron microscopy
PE	Polyethylene
SCB	Short chain branched
Me	Molecular weight between entanglements
Bst	p-(3-butenyl) styrene
Mw	Molecular weight (g/mol)
MFR	Melt flow ratio

MFI	Melt flow index
PODIC	Peroxydicarbonates
d	Interplanar distance (nm)
λ	Wavelength (nm)
2θ	Angle of diffraction ($^{\circ}$)
Δc_p	Heat capacity (J)
NMR	Nuclear magnetic resonance

LIST OF FIGURES

<i>Fig. 1: Various kinds of nucleation</i>	14
<i>Fig. 2: Polymer single lamellae [11]</i>	16
<i>Fig. 3: Maltese cross patterns [13]</i>	17
<i>Fig. 4: Schematic development of spherulites growth [11]</i>	17
<i>Fig. 5: Isotactic polypropylene [24]</i>	21
<i>Fig. 6: Syndiotactic polypropylene [24]</i>	21
<i>Fig. 7: Atactic polypropylene [24]</i>	22
<i>Fig. 8: Unoriented powder WAXD patterns for different forms in iPP crystals [19]</i>	22
<i>Fig. 9: Crystal structure of α-form of iPP [12]</i>	23
<i>Fig. 10: Crystal structure of β-form of iPP [12]</i>	24
<i>Fig. 11: Four unit cells of the γ-form of iPP according to the nonparallel chain packing model of Meille et al. [28]</i>	25
<i>Fig. 12: Preparation of LCP-PP by using heterogeneous catalysts [2]</i>	28
<i>Fig. 13: LCB-PP by radical reaction in iPP below 80 °C in inert atmosphere [32]</i>	29
<i>Fig. 14: LCB-PP by radical reaction on iPP at higher temperatures in presence of monomer [32]</i>	29
<i>Fig. 15: Conversion of the linear iPP structure into a LCB material [32]</i>	30
<i>Fig. 16: General formula of PODIC [35]</i>	31
<i>Fig. 17: The Bragg diffracting condition. Difference in path length between successive rays is $2d \sin \Theta$ [42]</i>	35
<i>Fig. 18: Schematic diagram of scanning electron microscope [45]</i>	37
<i>Fig. 19: Typical polymer DSC thermogram [46]</i>	38
<i>Fig. 20: Schematic diagram of differential scanning calorimetry [48]</i>	39
<i>Fig. 21: Instrument for the measurement of pvT behaviour [50]</i>	44
<i>Fig. 22: Rotary microtome Leica 2255 [51]</i>	45
<i>Fig. 23: Diffractometer X'PERT PRO MPD</i>	46
<i>Fig. 24: Differential scanning calorimeter Perkin-Elmer Pyris 1</i>	47
<i>Fig. 25: Scanning electron microscope Vega-II LMU [52]</i>	47
<i>Fig. 26: Compressive measurement INSTRON 8871</i>	48
<i>Fig. 27: The dependence of specific volume on temperature for PP crystallized under different pressures</i>	51

<i>Fig. 28: The dependence of specific volume on temperature for LCB-PP crystallized under different pressures</i>	51
<i>Fig. 29: The dependence of specific volume on temperature for c-PP crystallized under different pressures</i>	52
<i>Fig. 30: Crystallization temperatures of PP, LCB-PP, and c-PP crystallized under different pressures</i>	52
<i>Fig. 31: Diffractograms of PP samples crystallized at elevated pressure</i>	54
<i>Fig. 32: Diffractograms of LCB-PP samples at elevated pressure</i>	55
<i>Fig. 33: Diffractograms of c-PP crystallized at elevated pressure</i>	55
<i>Fig. 34: The content of γ-form of PP, c-PP, and LCB-PP crystallized at elevated pressure</i>	56
<i>Fig. 35: The dependence of crystallinity of PP, c-PP, and LCB-PP crystallized at elevated pressure</i>	56
<i>Fig. 36: Melting thermograms of PP crystallized at elevated pressure</i>	59
<i>Fig. 37: Melting thermograms of LCB-PP crystallized at elevated pressure</i>	59
<i>Fig. 38: Melting thermograms of c-PP crystallized at elevated pressure</i>	60
<i>Fig. 39: The evolution of melting temperature at elevated pressure</i>	60
<i>Fig. 40: The evolution of total enthalpy of melting at elevated pressure</i>	61
<i>Fig. 41: Morphology of PP, LCB-PP, and c-PP samples crystallized under different pressures by SEM (magnification 1 000x)</i>	63
<i>Fig. 42: Morphology of PP, LCB-PP, and c-PP samples crystallized under different pressures by SEM (magnification 2 000x)</i>	64
<i>Fig. 43: Morphology of LCB-PP crystallized at elevated pressure.</i>	65
<i>Fig. 44: The dependence of compressive stress at tensile strength on elevating pressure</i>	67
<i>Fig. 45: The dependence of compressive strain at tensile strength on elevating pressure</i>	68
<i>Fig. 46: The dependence of Modulus (automatic) on elevating pressure</i>	69

LIST OF TABLES

<i>Tab. 1: Properties of isotactic PP, syndiotactic PP and atactic PP [29]</i>	26
<i>Tab. 2: Mechanical properties of modified polypropylene material with long chain branches compared to linear polypropylene with identical melt flow rate [36].....</i>	33
<i>Tab. 3: Physical properties of LCB-PP Daploy WB130HMS</i>	42
<i>Tab. 4: Physical properties of PP homopolymer HC600TF</i>	43
<i>Tab. 5: Physical properties of PP homopolymer Borclean HB300BF.....</i>	43
<i>Tab. 6: Crystallization temperatures of PP, LCB-PP, and c-PP crystallized under different pressures</i>	50
<i>Tab. 7: The relative content of γ-form and crystallinity of PP, LCB-PP, and c-PP crystallized under different pressures (%)</i>	53
<i>Tab. 8: Melting temperature ($^{\circ}$C) and total enthalpy of melting (J/g) of PP, LCB-PP, and c-PP crystallized at elevated pressure</i>	58
<i>Tab. 9: Compressive stress at tensile strength for PP, LCB-PP, and c-PP crystallized at elevated pressure</i>	67
<i>Tab. 10: Compressive strain at tensile strength for PP, LCB-PP, and c-PP crystallized at elevated pressure</i>	68
<i>Tab. 11: Modulus (automatic) for PP, LCB-PP, and c-PP crystallized at elevated pressure</i>	69

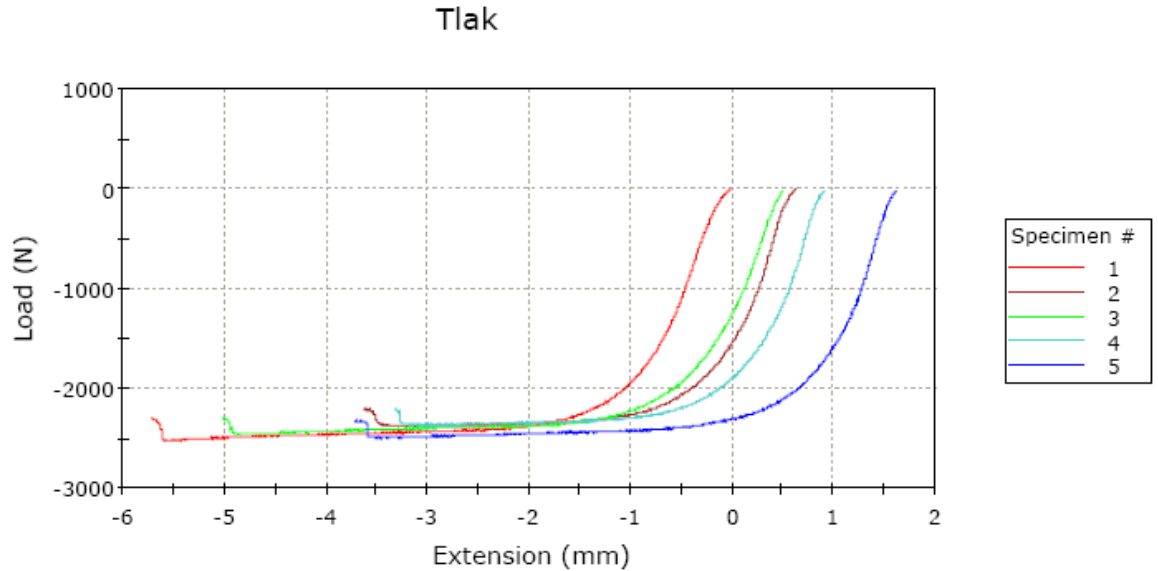
LIST OF EQUATIONS

(1) Avrami equation.....	18
(2) Avrami equation-logarithmic form.....	18
(3) Bragg equation.....	35
(4) Formula for compressive test speed.....	40

LIST OF APPENDICES

Appendix 1: Example of compressive testing results (polypropylene homopolymer HC600TF crystallized at pressure 20 MPa)

Appendix 1: Example of compressive testing results (polypropylene homopolymer HC600TF crystallized at pressure 20 MPa)



	Diameter (mm)	Anvil height (mm)	Area (cm ²)
1	7.69000	15.40000	0.46445
2	7.70000	15.80000	0.46566
3	7.67000	15.35000	0.46204
4	7.65000	15.46000	0.45963
5	7.67000	15.90000	0.46204
Mean	7.67600	15.58200	0.46277
Maximum	7.70000	15.90000	0.46566
Minimum	7.65000	15.35000	0.45963
Standard Deviation	0.01949	0.25024	0.00235
Coefficient of Variation	0.25396	1.60595	0.50788

	Compressive extension at Yield (Zero Slope) (mm)	Compressive load at Yield (Zero Slope) (N)	Compressive strain at Yield (Zero Slope) (mm/mm)
1	5.47299	2527.72808	0.35539
2	3.48789	2389.17291	0.22075
3	5.42609	2462.90028	0.35349
4	3.90641	2374.96734	0.25268
5	4.53852	2501.65343	0.28544
Mean	4.56638	2451.28441	0.29355
Maximum	5.47299	2527.72808	0.35539
Minimum	3.48789	2374.96734	0.22075
Standard Deviation	0.88889	67.44949	0.06011
Coefficient of Variation	19.46602	2.75160	20.47678

	Compressive stress at Yield (Zero Slope) (MPa)	Load at Yield (Zero Slope) (N)	Strain 1 at Yield (Zero Slope) (mm/mm)
1	54.42367	-2527.72808	-----
2	51.30696	-2389.17291	-----
3	53.30479	-2462.90028	-----
4	51.67077	-2374.96734	-----
5	54.14353	-2501.65343	-----

	Compressive stress at Yield (Zero Slope) (MPa)	Load at Yield (Zero Slope) (N)	Strain 1 at Yield (Zero Slope) (mm/mm)
Mean	52.96994	-2451.28441	-----
Maximum	54.42367	-2374.96734	-----
Minimum	51.30696	-2527.72808	-----
Standard Deviation	1.41917	67.44949	-----
Coefficient of Variation	2.67919	-2.75160	-----

	Compressive extension at Tensile Strength (mm)	Compressive load at Tensile Strength (N)	Compressive strain at Tensile Strength (mm/mm)
1	5.54342	2524.33836	0.35996
2	3.24156	2382.19261	0.20516
3	5.43087	2458.40728	0.35380
4	4.00264	2372.11525	0.25890
5	4.63195	2500.38087	0.29132
Mean	4.57009	2447.48688	0.29383
Maximum	5.54342	2524.33836	0.35996
Minimum	3.24156	2372.11525	0.20516
Standard Deviation	0.97200	68.49709	0.06530
Coefficient of Variation	21.26879	2.79867	22.22518

	Compressive stress at Tensile Strength (MPa)	Load at Tensile Strength (N)	Strain 1 at Tensile Strength (mm/mm)
1	54.35068	-2524.33836	-----
2	51.15706	-2382.19261	-----
3	53.20755	-2458.40728	-----
4	51.60871	-2372.11525	-----
5	54.11598	-2500.38087	-----
Mean	52.88800	-2447.48688	-----
Maximum	54.35068	-2372.11525	-----
Minimum	51.15706	-2524.33836	-----
Standard Deviation	1.44760	68.49709	-----
Coefficient of Variation	2.73/11	-2.79867	-----

	Modulus (Tangent 0 mm) (MPa)	Extension at Yield (Zero Slope) (mm)	Extension at Tensile Strength (mm)
1	964.60117	-5.47299	-5.54342
2	1227.89860	-3.48789	-3.24156
3	987.64827	-5.42609	-5.43087
4	1188.23768	-3.90641	-4.00264
5	1204.07489	-4.53852	-4.63195
Mean	1118.49212	-4.56638	-4.57009
Maximum	1227.89860	-3.48789	-3.24156
Minimum	964.60117	-5.47299	-5.54342
Standard Deviation	121.66093	0.88889	0.97200
Coefficient of Variation	10.87723	19.16602	21.26879

	Modulus (Automatic) (MPa)
1	758.06709
2	918.44469
3	705.41375
4	860.94937
5	807.73532
Mean	814.12205
Maximum	918.44469
Minimum	705.41375
Standard Deviation	87.10561
Coefficient of Variation	10.69933